ELSEVIER

Contents lists available at ScienceDirect

## Quaternary Geochronology

journal homepage: www.elsevier.com/locate/quageo





# Meteoric <sup>10</sup>Be speciation in subglacial sediments of East Antarctica

Eiríka Ö. Arnardóttir<sup>a</sup>, Joseph A. Graly<sup>b,\*</sup>, Kathy J. Licht<sup>a</sup>, David L. Bish<sup>c</sup>, Marc W. Caffee<sup>d</sup>

- <sup>a</sup> Indiana University Purdue University Indianapolis, Earth Sciences, Indianapolis, IN, USA
- <sup>b</sup> Northumbria University, Geography and Environmental Sciences, Newcastle Upon Tyne, UK
- <sup>c</sup> Indiana University, Earth and Atmospheric Sciences, Bloomington, IN, USA
- <sup>d</sup> Purdue University, Physics and Astronomy, West Lafayette, IN, USA

#### ARTICLE INFO

# Keywords: Meteoric <sup>10</sup>Be Antarctic ice sheet Subglacial processes Chemical weathering Sequential extractions Clays

#### ABSTRACT

A sequential chemical extraction procedure was developed and tested to investigate the utility of meteoric <sup>10</sup>Be as a tracer for authigenic mineral formation beneath the East Antarctic Ice Sheet. Subglacial meltwater is widely available under the Antarctic Ice Sheet and dissolved gases within it have the potential to drive chemical weathering processes in the subglacial environment. Meteoric <sup>10</sup>Be is a cosmogenic nuclide with a half-life of 1.39·106 years that is incorporated into glacier ice, therefore its abundance in the subglacial environment in Antarctica is meltwater dependent. It is known to adsorb to fine-grained particles in aqueous solution, precipitate with amorphous oxides/hydroxides, and/or be incorporated into authigenic clay minerals during chemical weathering. The presence of  $^{10}$ Be in chemical weathering products derived from beneath the ice therefore indicates chemical weathering processes in the subglacial environment. Freshly emerging subglacial sediments from the Mt. Achernar blue ice moraine were subject to chemical extractions where these weathering phases were isolated and <sup>10</sup>Be concentrations therein quantified. Optimization of the phase isolation was developed by examining the effects of each extraction on the sample mineralogy and chemical composition. Experiments on <sup>10</sup>Be desorption revealed that pH 3.2-3.5 was optimal for the extraction of adsorbed <sup>10</sup>Be. Vigorous disaggregation of the samples before grain size separations and acid extractions is crucial due to the incorporation of the nuclide in clay minerals and its preferential absorption to clay-sized particles. <sup>10</sup>Be concentrations of 2-22·10<sup>7</sup> atoms·g<sup>-1</sup> measured in oxides and clay minerals in freshly emerging sediments strongly indicate subglacial chemical weathering in the catchment of the Mt. Achernar moraine. Based on total <sup>10</sup>Be sample concentrations, local basal melt rates, and 10Be ice concentrations, sediment-meltwater contact in the subglacial environment is on the order of thousands of years per gram of underlying fine sediment. Strong correlation (R = 0.97) between <sup>10</sup>Be and smectite abundance in the sediments supports authigenic clay formation in the subglacial environment. This suggests meteoric <sup>10</sup>Be is a useful tool to characterize subglacial geochemical weathering processes under the Antarctic Ice Sheet.

### 1. Introduction

Chemical weathering of Earth materials plays a key role in major global geochemical cycles such as the carbon and sulfur cycles that regulate the Earth's climate (Kump et al., 2000; Petsch, 2014; Relph et al., 2021), and the iron and phosphorous cycles that deliver essential nutrients to Earth's oceans (Filippelli, 2008; Raiswell and Canfield, 2012). A growing body of evidence suggests that the subglacial environment is an active site of chemical weathering both in Antarctica (Graly et al., 2020; Michaud et al., 2016; Skidmore et al., 2010; Wadham et al., 2012) and globally (Graly et al., 2017; Li et al., 2022; Torres et al.,

2017). However, considerable uncertainty remains over the exact chemical reaction pathways dominant in various subglacial environments, the ligands produced, and the timescales involved.

Generally, subglacial chemical weathering occurs when the atmospheric gases within glacial meltwater interact with sediments formed from grinding and fracturing of rock at the ice bed (Anderson, 2005; Graly et al., 2017; Tranter et al., 2002). With at least 55% of grounded ice in Antarctica at the pressure melting point, most subglacial water on the Antarctic continent is basal meltwater sourced by geothermal and strain heating; most of East Antarctica experiences melt rates between 2 and 6 mm·a<sup>-1</sup>, but with substantially higher melt in high ice flux regions

E-mail address: joseph.graly@northumbria.ac.uk (J.A. Graly).

<sup>\*</sup> Corresponding author.

#### (Pattyn, 2010).

Here we examine the distribution of the cosmogenic nuclide meteoric 10Be among mineral species as a tracer for subglacial mineral formation at Mt. Achernar Moraine, a blue ice moraine in the central Transantarctic Mountains. At blue ice moraines scattered across the continent, particularly along the Transantarctic Mountains (Palmer et al., 2012), the overlying ice is trapped and ablated away through sublimation (Bintanja, 1999; Kassab et al., 2020), allowing subglacial sediments to reach the surface of the ice sheet and become accessible for sampling. Blue ice moraines are therefore repositories of material representative of the otherwise ice-covered subglacial environment. Rockfall from the surrounding topography can also contribute to sediment accumulation at blue ice moraines. However, the material at Mt. Achernar Moraine bears strong evidence of subglacial origin rather than rockfall (Bader et al., 2017; Graly et al., 2020; Kaplan et al., 2022; Kassab et al., 2020). Subglacial chemical weathering is evidenced at the site by abundant chemical weathering products and a decline in magnetic susceptibility compared with the source rock (Graly et al., 2020).

Meteoric <sup>10</sup>Be is a cosmogenic nuclide with a half-life of 1.39·10<sup>6</sup> years (Korschinek et al., 2010). It is formed by spallation reactions when galactic cosmic rays interact with atoms in the atmosphere (primarily <sup>14</sup>N and <sup>16</sup>O; Fig. 1) (Morris et al., 2002). Use of meteoric <sup>10</sup>Be as a tracer for soil and sediment processes has largely been focused on temperate environments but is increasingly gaining momentum in the field of glacial studies (Graly et al., 2018a; Schiller et al., 2014; White et al., 2019). Antarctica has been glaciated for >30 Ma (Barrett et al., 2007; DeConto and Pollard, 2003; Pollard and DeConto, 2009; Zachos and

Kump, 2005), well beyond the applicability of the meteoric <sup>10</sup>Be signal. Any meteoric <sup>10</sup>Be deposited on the continental interior prior to glaciation is therefore depleted. Most of the <sup>10</sup>Be that is currently found on the continent (deposited in the past 10 Ma) has settled on and accumulated in the ice sheet.

<sup>10</sup>Be deposition in Antarctica is heavily dependent on snow accumulation, with higher concentrations accumulating with low snowfall, and lower concentrations when snowfall is higher. The climatological effect on meteoric  $^{10}\mathrm{Be}$  concentrations in ice is evident in ice core records from Dome C and Vostok in Antarctica's deep interior where <sup>10</sup>Be concentrations from the late Pleistocene are higher than concentrations from the Holocene by a factor of 2–3, despite <sup>10</sup>Be flux being relatively constant during those periods (Raisbeck et al., 1987; Yiou et al., 1985). The Mt. Achernar Moraine ice is sourced from the polar plateau and has stable isotopes signatures that indicate formation during the Pleistocene (Graly et al., 2018c, Fig. 2). Ice core records from Vostok, which is the closest core to the source location for Mt. Achernar Moraine's ice, show meteoric <sup>10</sup>Be concentrations of ~2·10<sup>5</sup> atoms·g<sup>-1</sup> during Pleistocene periods (Raisbeck et al., 1990). Subglacial melt rates at the site are approximately 7.5 mm·a<sup>-1</sup> (Graly et al., 2020), giving an effective deposition rate of approximately 1.35·10<sup>5</sup> atoms·cm<sup>-2</sup>·a<sup>-1</sup> in the subglacial environment.

In contrast, *in situ*  $^{10}$ Be, produced by spallation reactions within the structures of minerals exposed on the Earth's surface, forms at a far lower rate and would have minimal abundances in newly exposed glacial sediments. It is produced at 3.60–3.82 atoms· $g_{quartz}^{-1}$  in Antarctica (Kaplan et al., 2011). *In situ*  $^{10}$ Be production exponentially

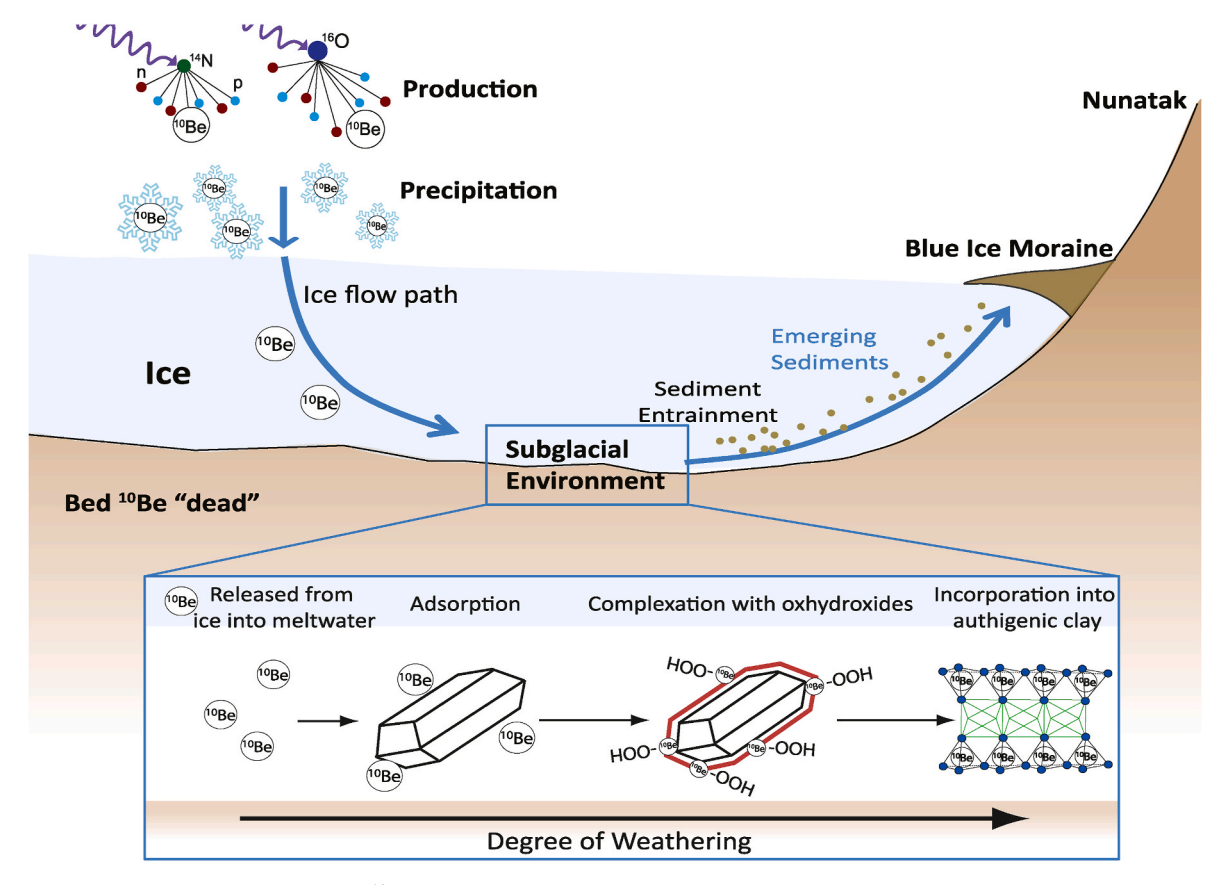


**Fig. 1.** The conceptual model of the study: meteoric <sup>10</sup>Be is produced in the atmosphere through the spallation of oxygen and nitrogen by galactic cosmic rays; it is delivered to the ice surface by a mix of wet and dry deposition; The downward ice flux delivers <sup>10</sup>Be to the subglacial environment, finally emerging at the surface at a blue ice moraine. Ice cover has prevailed for >30 Ma, meaning that any detectable meteoric <sup>10</sup>Be concentrations in the freshly emerging sediments at the moraine must have accumulated via chemical processes in the subglacial environment after being released from the ice into meltwater. Adsorbed <sup>10</sup>Be therefore indicates the presence of meltwater, <sup>10</sup>Be in oxides or oxyhydroxides would indicate the precipitation of those phases, and <sup>10</sup>Be in clay structures would indicate the authigenic formation of clay minerals in the subglacial environment. Subglacial sediments become entrained in the basal ice layers and emerge on the surface in blue ice areas due to high sublimation rates and upward flow trajectories of the ice.

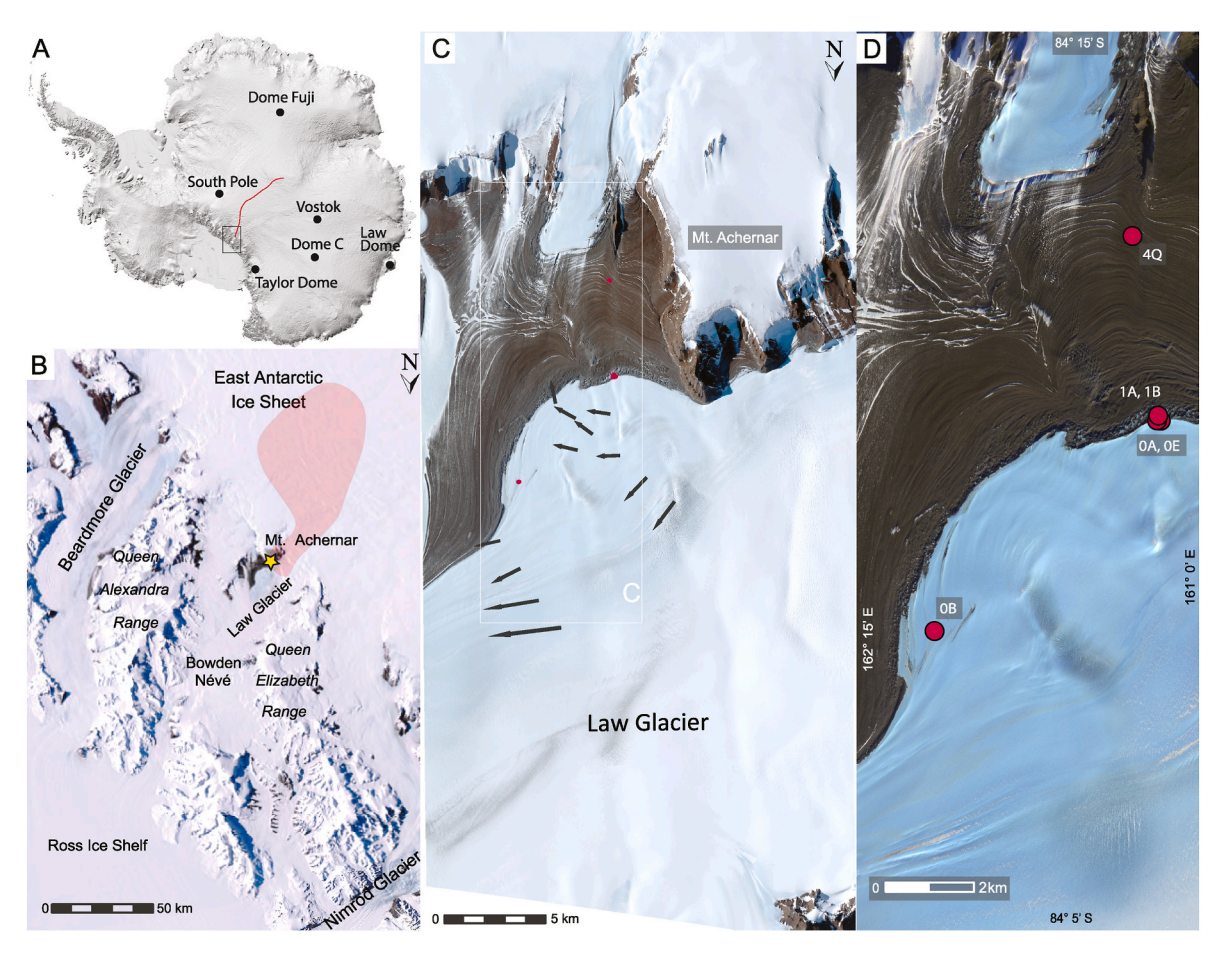


Fig. 2. A) The site location on a continental scale, in reference to major East Antarctic ice core sites. The red line indicates the approximate course of ice towards Mt. Achernar Moraine. B) Mt. Achernar Moraine in the Central Transantarctic Mountains, Mt. Achernar is marked with a yellow star, and the inferred  $\sim$ 4000 km<sup>2</sup> catchment area of the Mt. Achernar Moraine sediments from Graly et al., 2018c is shaded in red. C) Sampling locations at the Mt. Achernar Moraine. GPS data from Kassab et al., 2020 are included as black arrows which indicate the flow direction and relative magnitude of the ice flow velocity, which is fastest at  $\sim$ 25 my<sup>-1</sup>. D) Inset of sampling locations. Sample 4Q was collected  $\sim$ 2 km inward of the active margin of the moraine, where samples 1A, 1B, 0A and 0E were collected. Sample 0B was collected from a debris band outside of the moraine margin. Imagery ©2014 Digital Globe, Inc. provided by the Polar Geospatial Center (St. Paul, Minnesota, USA).

declines as a function of basal ice overburden (Corbett et al., 2021). The ablation rate at the ice margin is 0.7 cm·a<sup>-1</sup> (Kassab et al., 2020), allowing for order of 1000 years of appreciable in situ <sup>10</sup>Be production as debris emerges. Integrating the production of the isotope through the emerging ice column and correcting for the shielding effects of ice,  ${<}1000 \; atoms {\cdot} g_{quartz}^{-1}$  would be present in the emerging sediments. With freshly-emerging till density at 1.8 g·cm<sup>-3</sup> and ~25% quartz mineralogy (Graly et al., 2020), we would expect the emerging sediments to bear <500 in situ 10 Be atoms cm3. Though other minerals, such as feldspars, may also produce in situ <sup>10</sup>Be atoms (Zerathe et al., 2017), the quartz production is equivalent to the meteoric <sup>10</sup>Be accumulated in only 1 or 2 days in the subglacial environment. *In situ* <sup>10</sup>Be production and meteoric <sup>10</sup>Be deposition continue once the sediments are on the ice or moraine surface. However, the duration of surface exposure in fresh sediments is very small. Nitrate, an atmosphere produced salt, is below detection limits in our freshest subglacial sediments, indicating less than 100 years of atmospheric exposure (Graly et al., 2022). In situ cosmogenic isotope exposure ages in freshly emerging cobbles range from 52 to 79 years at moraine margin (Kaplan et al., 2022), consistent with the salt data. A detectable meteoric  $^{\hat{10}}$ Be signal in these sediments could only indicate the accumulation of the nuclide into those sediments from the melt of overlying ice in the subglacial environment.

The speciation of meteoric  $^{10}$ Be in the weathering environment is fundamentally controlled by beryllium's atomic properties. Be $^{2+}$  has the smallest radius of all metal ions (0.27 Å) and a high charge-to-radius

ratio, making it a strong Lewis acid (electron pair acceptor). As a highly polarizing element, it has a strong affinity for oxygen and thus is capable of orienting water molecules around itself in a positively charged hydrosphere (Everest, 1964; Hawthorne and Huminicki, 2002). In minerals, Be exists exclusively in tetrahedral coordination with oxygen (Hawthorne and Huminicki, 2002). Be<sup>2+</sup> substitution into octahedral sites would cause structural collapse (Wang et al., 2017) and breaking of strong bonds to facilitate tetrahedral coordination of the ion (Buchner, 2020). Beryllium can form as a mineral oxide or hydroxide, or coordinate in aluminosilicates as either an essential cation that cannot be replaced by other cations due to its uniquely small size, or as a substituting cation, commonly for Si and Al, in tetrahedral sites in silicate minerals (Hawthorne and Huminicki, 2002; Vesely et al., 2018). Because of their similar ionic radii, Be<sup>2+</sup> can substitute for the Si<sup>4+</sup> ion (0.39 Å) within SiO<sub>4</sub> tetrahedra in silicate minerals (Beus, 1956; Rankama and Sahama, 1950). The chemical behavior of Al<sup>3+</sup> is similar to Be<sup>2+</sup> due to similar charge densities, electronegativities and charge-to-size ratio of the two ions; beryllium replacement of aluminum in aluminosilicates can occur in the presence of a hydroxide (Beus, 1956). Mn and Mg are also major cations for which beryllium is known to substitute (Everest et al., 1973; Ryan, 2002). As a lithophile element, Be preferentially partitions into silicate minerals as opposed to sulfides or metals. It has been found to show preference for clay minerals over Fe-oxides once weathered from silicates and available in solution (Beus, 1956; Lum and Gammon, 1985).

In the context of chemical weathering, Be can form in three fundamental states: as a cation coordinated within a hydrosphere capable of sorbing to a negatively charged surface; as an oxide or hydroxide precipitated via hydrolysis or oxidation reactions; or as a substituting cation in a newly precipitated aluminosilicate, typically a clay mineral (Barg et al., 1997; Wittmann et al., 2012; You et al., 1989).

Aqueous Be has a strong propensity to adhere to fine-grained particles, with a partition coefficient ( $K_d$ ) on the order of  $\sim 10^5 \text{ ml} \cdot \text{g}^{-1}$  at neutral conditions (pH  $\geq$  6) (You et al., 1989). Adsorption experiments, with equilibration times from 3 min up to 108 days (Li et al., 1984; Nyffeler et al., 1984; You et al., 1989), have shown that the sorption process takes place in two steps. The first step occurs within the first day, where K<sub>d</sub> increases rapidly, and is thought to involve the easily accessible exchange sites of the solids being occupied by Be. Kd increases at a slower rate in the second step, which might indicate that the exchange of Be takes place through slow diffusion toward less accessible sites, possibly inside the interlayers of clay mineral structures (Nyffeler et al., 1984; You et al., 1989). The reversibility of the adsorption process has been demonstrated with desorption experiments and appears to happen in two steps as described for the adsorption process, with a rapid decrease of K<sub>d</sub> in the first day and then slowly decreasing K<sub>d</sub> values after that (Li et al., 1984; Nyffeler et al., 1984; You et al., 1989). Sorbed Be concentrations correlate with cation exchange capacity (CEC) (Boschi and Willenbring, 2021). However, low CEC clays such as illite will desorb Be less readily and are less sensitive to water chemistry effects (Boschi and Willenbring, 2016; Kabata-Pendias and Pendias, 1984).

During chemical weathering, Be frequently precipitates with Fe and Al to form oxides, hydroxides, and oxyhydroxides (Barg et al., 1997; Jungers et al., 2009; McHargue and Damon, 1991; Nyffeler et al., 1984; Takahashi et al., 1998). The association between meteoric <sup>10</sup>Be and these oxyhydroxide phases is supported by a frequent correlation of the isotope with dithionite-citrate extractable Al, and to a lesser degree, extractable Fe (Graly et al., 2010; Jungers et al., 2009). The retention of beryllium in these phases is mainly controlled by the presence and amount of grain coatings, composed of HCl-extractable Fe, Mg, Ca and Mn phases (Singleton et al., 2016).

If <sup>10</sup>Be is available in the soil where new clay minerals form during rock weathering, it is incorporated into the authigenic clay mineral structures (Kabata-Pendias and Pendias, 1984). Barg et al. (1997) found that 42–92% of the <sup>10</sup>Be in the lower B and C horizons of the soil profiles in their study was contained within the structures of authigenic clays. Any Be sorbed or in other authigenic phases was removed in a 0.5 M HCl leach (Barg et al., 1997), strongly suggesting that the remaining <sup>10</sup>Be was coordinated in Si tetrahedral sites. <sup>10</sup>Be uptake into authigenic clay minerals is also strongly suggested in marine settings (Bernhardt et al., 2020).

The three main sediment fractions in which Be is known to exist adsorbed in aqueous systems, precipitated with oxides and oxyhydroxides, and incorporated into authigenic clay mineral structures are proposed as indicators for the degree of subglacial chemical weathering. For <sup>10</sup>Be to adsorb to the surface of the sediment particles, the Be would have to be released from the ice as it melted and come into contact with the sediment through the glacial melt water. Meteoric  $^{10}\mathrm{Be}$ measured in oxides or oxyhydroxides would indicate the precipitation of those species in the subglacial environment. Lastly, if  $^{10}$ Be is contained in clay structures, that would indicate the authigenic formation of clays in the subglacial environment. In this study, we develop and test laboratory techniques for isolating these three phases in the context of Antarctic subglacial sediments. The relative distribution of <sup>10</sup>Be between the three phases could elucidate the chemical weathering activity under the ice, i.e. the higher degree of complexation of <sup>10</sup>Be, the higher the degree of weathering (Fig. 1).

## 2. Study site

The bedrock exposed near Mt. Achernar Moraine consists of Permo-

Triassic strata, composed of glacial, alluvial, and shallow marine sedimentary rocks; this stratigraphic sequence is part of the Beacon Supergroup (Barrett et al., 1986). The Beacon Supergroup is intruded by mafic sills of the expansive Ferrar Dolerite (Isbell, 1990). Studies conducted elsewhere in the Transantarctic Mountains have documented local contact metamorphism caused by the Ferrar intrusions and burial diagenesis resulted in the formation of illite, chlorite and zeolite cements (Bernet and Gaupp, 2005). The sediments analyzed in this study are sourced from the local bedrock formations or similar subglacial bedrock sources up glacier (Bader et al., 2017; Graly et al., 2018c, 2020).

Mt. Achernar Moraine is fed by Law Glacier, which flows from the East Antarctic Ice Sheet between the Queen Alexandra and Queen Elizabeth Ranges of the central Transantarctic Mountains. Mt. Achernar is the first exposed nunatak that Law Glacier encounters as it flows from the polar plateau towards the Ross Embayment (Fig. 2B). The regional subglacial topography has been >1000 m from the formation of the Antarctic Ice Sheet through the present (Jamieson et al., 2010; Paxman et al., 2019), and modeling and offshore studies suggest a persistent Antarctic Ice Sheet over >10 Ma in the region (DeConto and Pollard, 2003; Pollard and DeConto, 2009; Shakun et al., 2018; Wilson et al., 2012). The potential for pre- and interglacial exposure, inheritance, and weathering at the site is therefore low.

Law Glacier encounters Mt. Achernar as a barrier in its path, where a blue ice area has formed at an elevation of ~1700-1900 m above sea level. Together, the flow of Law Glacier along Mt. Achernar and sublimation at the blue ice area cause the upward ice-flow trajectories of Law Glacier along the nunatak and the eventual exposure of subglacially derived sediments at the Mt. Achernar Moraine (Fig. 2C) (Bader et al., 2017; Kassab et al., 2020). Modeled warm basal conditions (Pattyn, 2010) and stable isotope signatures of the ice in the catchment area suggest that the moraine's sediment is subglacially derived and was entrained by regelation, a warm-based process, with a catchment extending approximately 30-50 km upstream (Fig. 2B) (Graly et al., 2018c). Based on surface exposure ages (Kaplan et al., 2017, 2022) and boron concentrations (Graly et al., 2018b), lateral debris accumulation rates of the moraine range from 2 to > 40 m ka<sup>-1</sup> and vary over time, with higher accumulation rates occurring in colder climate conditions (Kassab et al., 2020). The approximate time since the entrainment of the sediments  $\sim$ 30-50 km upstream is estimated to be 95-135 ka and the emergence time from the glacial bed to the moraine surface approximately 35 ka (Kassab et al., 2020).

Mass balance calculations on the mineralogy and elemental composition of the <63 µm size fraction showed that 28% of the input to the site is from the Ferrar dolerite and 72% from sand- and siltstones of the Fairchild and Mackellar Formations of the Beacon Supergroup (Graly et al., 2020). The mineralogical and chemical composition of the subglacially derived <63 µm fraction of sediment freshly emerging at the moraine margin indicate significantly more weathering products than the representative source rock. This manifests as losses in feldspar and pyroxene and enrichment in smectite and kaolinite, calcite, zeolites, amorphous Si, and other amorphous oxides or oxyhydroxides (Graly et al., 2020). Magnetic susceptibility measurements found significant magnetite depletion in the sediments relative to the source rock, suggesting the oxidation of magnetite from the source rock (Graly et al., 2020). Many of these alteration products (i.e. clay minerals, oxides, and oxyhydroxides) are potential beryllium hosts, with meteoric 10Be in their crystal structures expected only if they formed in the subglacial environment.

## 3. Methods

Glacial sediment samples were collected from Mt. Achernar Moraine during the 2010 and 2015 field seasons. A diverse range of sediments were either collected directly from ablating ice or from the first crests on the active margin of the moraine; we define these as freshly emerging sediments. Additionally, samples exposed on the moraine surface for up

to 550 ka were collected along a 6.5 km transect across the moraine (Bader et al., 2017; Kaplan et al., 2017). Samples were collected using chemically inert, plastic scoops and sample bags. Five samples of the freshly emerging sediments (1A, 1B, 0A, 0B, 0E) and one sample (4Q) with a 550 ka year exposure history (Kaplan et al., 2017), collected about 2 km inward of the moraine margin, were included in this study (Fig. 2D).

Dry samples (i.e. 4Q) were stored at room temperature, and samples wet from ablating ice (i.e. the other 5) were stored in a refrigerator at  $4^{\circ}$ C. Moisture was removed from wet samples by freeze drying. Dry samples were sieved through a 2 mm mesh sieve to separate gravel-sized grains from smaller grains. Gravel-sized particles were hand-picked from wet samples.

Sequential chemical extractions were employed to isolate three sediment fractions in which meteoric <sup>10</sup>Be is likely found: 1) adsorbed; 2) reducible oxides and oxyhydroxides; and 3) residual clay and silicate fractions. Sequential extractions are a technique where solid samples are subject to a series of progressively stronger acids, each designed to selectively dissolve specific components of the sediment particles (Tessier et al., 1979; Wiederhold et al., 2007). Sequential extraction schemes typically involve the chemical separation of trace elements into: 1) fractions soluble in water; 2) exchangeable and/or acid soluble fractions (elements associated with carbonates); 3) reducible (mainly Fe and Mn oxides); 4) oxidizable (metals bound to organic matter); and 5) residual/silicate fractions (crystalline-bound trace elements) (Du Laing, 2011). Our approach here was modified to exclude parts of the sequence

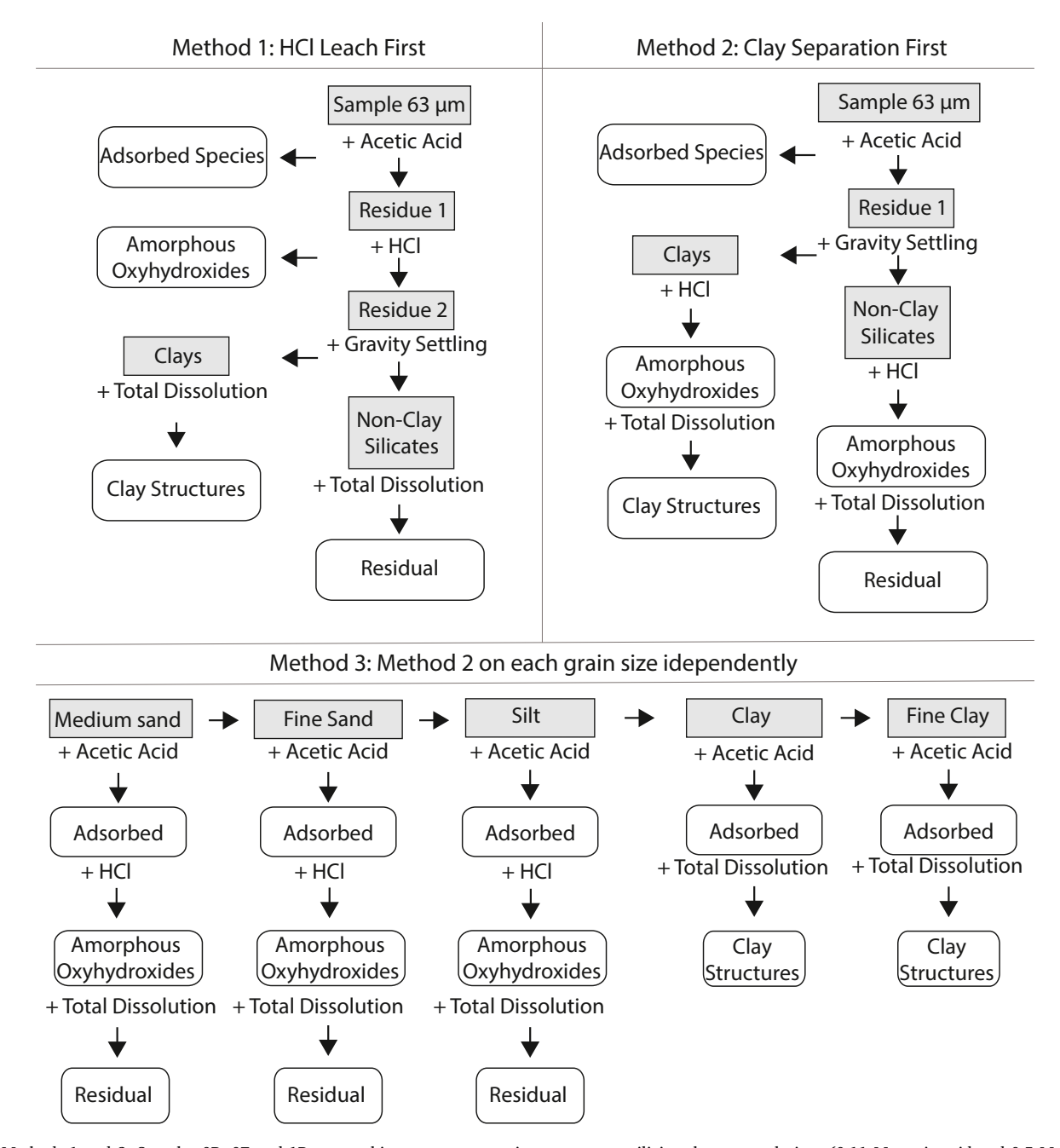


**Fig. 3.** Methods 1 and 2: Samples 0B, 0E and 1B were subject to two extraction sequences utilizing the same solutions (0.11 M acetic acid and 0.5 M HCl) and digestion procedures, but with clay separations at different stages in the sequence. In method 1, the clays were separated after the HCl extraction and in method 2, the clays were separated before the HCl extraction. Method 3: Samples 0A, 0B and 1A were subjected to sequential extractions after being separated into five different size fractions to investigate the effects of grain size on <sup>10</sup>Be distribution.

that are unlikely to bind significant beryllium, namely acid soluble and oxidizable phases (Wittmann et al., 2012).

The three defined sediment phases need to be isolated as accurately and completely as possible in order to utilize <sup>10</sup>Be concentrations therein as a proxy for subglacial chemical weathering. Acetic acid (CH<sub>3</sub>COOH) in 0.11 M concentration was used to target adsorbed species and carbonate minerals. The dry samples were placed in plastic tubes and 40 ml of the 0.11 M CH<sub>3</sub>COOH added. After shaking the samples completely into suspension, the tubes were placed on a vibrating table for 16 h. The samples were centrifuged at 3400×g relative centrifugal force for 15 min, and the acid and the dissolved components therein (the leachate) was then decanted into new tubes and stored for future analyses. Thirty ml of deionized water were then added to the samples as a rinse, which were shaken completely into suspension and left on a vibrating table for 2-h to rinse, then centrifuged and the supernatant water discarded. This was followed by a 24-h leach with 0.5 M hydrochloric acid (HCl), which was used to dissolve amorphous/non-crystalline phases such as oxides and oxyhydroxides (Wittmann et al., 2012), following the same procedures as for the acetic acid extraction. What remained of the samples after the acetic and hydrochloric acid extractions was totally dissolved in various mixtures of HCl, nitric acid (HNO3), and hydrofluoric acid (HF) using microwave digestion.

Within this sequential extraction framework, we performed three separate experiments to explore the effects of methods choices on the extraction. This included tests on the CH<sub>3</sub>COOH extraction, tests on the HCl extraction, and tests examining the effects of grain size.

The effects of the 16-h CH $_3$ COOH extraction on the adsorbed species and oxide and oxyhydroxide grain coatings were tested in all 6 samples by applying four different concentrations: 0.05 M, 0.11 M, 0.22 M and 0.44 M. The pH of each solution was measured before adding 1 g of sample in the <63  $\mu m$  size fraction, immediately after sample addition, and every 2 h for the remainder of the extraction, using an Oakton 700 pH meter. Chemical data (ICP-OES analysis) were used to assess which species dissolved in each solution and to determine the ideal pH levels to target adsorbed species.

To determine the effects of 0.5 M HCl on clay minerals, ~1 g drysieved aliquots in the <63 µm size fraction of samples 0B, 0E and 1B were subjected to two different sequential extraction methods (Fig. 3, methods 1 & 2). Both methods were the same in all regards except for the timing of clay separations by gravity settling. All samples were leached in 0.11 M CH3COOH for 16 h and water rinsed for 2 h, then leached in 0.5 M HCl for 24 h. Clays were separated after the HCl extraction in method 1 and before the HCl extraction in method 2. To separate the clays, Milli-Q water was added to the sample tube, the tube was agitated and placed in an ultrasonic bath for 3 min to suspend material, and it was then allowed to settle for 24 h to isolate  $<1~\mu m$ particles. The supernatant, sediment-bearing water was then separated and centrifuged down as a clay fraction. All samples were rinsed after the HCl leach, oven dried at 60°C, and weighed once they reached room temperature. A mixture of HF, HNO<sub>3</sub>, and HCl in the ratio 1:2:2 was used in the total dissolution process. The samples were shaken vigorously to ensure complete particle suspension, sonicated at 50 °C for 3 h, and then digested in a CEM corporation Microwave Digestion System. In an initial trial on a single sample (0B), but not subsequently, we included a hydroxylamine hydrochloride (NH2OH-HCl) leach between the HCl extraction and the separation of the clay fraction. This extraction followed the methods of Graly et al. (2020). The residual silt fraction was not analyzed by total dissolution during this initial trial.

Grain size dependency was investigated by separating each sample into different grain sizes using blending, sonication, wet sieving, and gravity-settling based on standard procedures according to Stoke's Law (Chipera et al., 1993; Tanner and Jackson, 1947). The terms used to describe the grain size fractions hereafter are operationally defined and therefore might not follow Wentworth grain size classification for grains  $<\!63~\mu m$ . After the initial 2 mm dry sieving, a  $\sim\!5$  g subsample of four samples (0A, 0B, 1A, 4Q) was weighed and disaggregated by mixing in a

Waring Blade BB340SK bar blender for 60 s and sonicated using a sonication probe from a Malvern Hydro MU unit for 10 min twice before grain size separation (Chipera et al., 1993). The samples were suspended in water in glass beakers for 10 min. The settled material was wet sieved with a 250  $\mu m$  sieve, yielding the size medium sand fraction, and a 63 um sieve, vielding the fine sand size fraction. Grains still in suspension after the 10-min settling were decanted with the water for a subsequent 1-h settling. Settled material from the 1-h settling was operationally defined as silt in this study. Suspended material after the 1-h settling was decanted and settled for another 15 h. Materials settled during the 15 h are referred to as coarse clay, and what was still in suspension is referred to as fine clay. By these operational definitions, coarse clay was not analyzed as clay in methods 1 and 2 (Fig. 3). Medium sand, fine sand, and silt fractions were centrifuged, and the water decanted. The water from the coarse and fine clay fractions was evaporated by leaving the samples in an oven at 62°C until only the moist clays were left. The remaining moisture in all samples was removed by freeze drying. The separated grain size fractions were then subjected to independent extraction procedures, with sand- and silt-sized fractions subjected to CH3COOH, HCl, and total dissolution leaches, and clay fractions omitting the HCl leach (Fig. 3C); this procedure is hereafter referred to as method 3.

Chemical and mineralogical effects of the sequential chemical extraction procedures were examined using ICP-OES (Inductively Coupled Plasma - Optical Emission Spectrometry) and X-ray powder diffraction (XRD) analyses to assess and optimize the efficacy of the phase isolation. Aliquots from each extraction were analyzed by ICP-OES and the results used to assess whether procedural adjustments were necessary. Sediment aliquots were analyzed before and after treatment to assess loss of mineral species. Comparability was achieved by subjecting a single sample, 0B, to all experiments. Changes in clay mineralogy were measured with a Bruker D8 Discover X-ray diffractometer. Clay mineral samples were prepared by suspending the fine clay fractions of the samples in water and pipetting on to a zerobackground slide where they would air-dry. After analysis, the samples were placed in a glycol chamber for 48 h and analyzed again to study the expandable clays within the samples. Clay mineral XRD scans were measured from  $2^{\circ}$  to  $30^{\circ}$   $2\theta$ .

All extracts and blanks were spiked with 250  $\mu$ l of a  $^9$ Be standard (1041  $\pm$  8 ppm) prepared at PRIME Lab, Purdue University (Batch number: 2014.10.20-Be). The weight of the sample and spike were recorded with a Mettler Toledo XS250DU weighing scale with 5 decimal points and repeatability of 0.05 mg. Beryllium was separated from the sample extracts by anion and cation-exchange column chromatography at the Tulane University Cosmogenic Nuclide Laboratory (TUCL) and PRIME Lab following standard procedures (Ditchburn and Whitehead, 1994; Ochs and Ivy-Ochs, 1997).  $^{10}$ Be was measured as a fraction of  $^9$ Be by accelerator mass spectrometer at PRIME Lab, along with KNSTD07 standards and processes blanks for each of the experiments.

## 4. Results

## 4.1. Acetic acid experiments

Acetic acid extractions at four different concentrations were used to assess the pH range at which adsorbed and carbonate-bound species, including  $^{10}\text{Be}$ , mobilize without significantly affecting other grain components. pH levels in the blank solution ranged from  $\sim\!2.45$  in 0.44 M extractions to  $\sim\!3$  in the 0.05 M extraction (Appendix A). Sample addition to the solution immediately dropped [H $^+$ ] by 40–90%. pH continued to increase for 4 h, then stabilized. Ultimately, [H $^+$ ] dropped by 64–95%. [H $^+$ ] dropped by 77–95% for the relatively calcite-rich samples, 1A and 4Q, whereas calcite-poor samples saw [H $^+$ ] declines of 64–80% (Appendix A).

Higher quantities of all elements, including meteoric <sup>10</sup>Be, were leached from all samples as pH decreased with increased acetic acid

input (Fig. 4). The most abundant element in the acetic acid leaches was Ca at 0.27–1.1% of the sample weight, with samples 1A and 4Q yielding up to two times more than the other samples. Mg, Si, Al and Fe were all at 0.30% or less, with Fe being the least abundant element. Si, Al and Fe all show similar patterns with decreased pH, namely small increases between 0.05 M and 0.11 M, corresponding to pH 3.7–3.3. Significant Si, Al and Fe yield occurred at pH < 3.2, corresponding to the 0.22 M solution. In the case of  $^9{\rm Be}$  and  $^{10}{\rm Be}$ , however, the difference between the elemental yield of 0.05 M and 0.11 M was significant, in some cases with a twofold increase in yield between the two concentrations. Solution pH between 3.2 and 3.5, corresponding to a concentration of 0.11 M for most samples, maximally desorbed  $^{10}{\rm Be}$  without significantly affecting other grain components.

## 4.2. HCl and clay mineral experiments

The effect of 0.5 M HCl on clay minerals was assessed by performing the HCl extraction either before (method 1) or after (method 2) the physical separation of clays (Fig. 3). More  $^{10}$ Be was measured in the clay and residual fractions in all samples from method 2, making the oxyhydroxide-bound  $^{10}$ Be a smaller fraction relative to method 1 (Fig. 5). In method 1, XRD patterns from the gravity-separated, clay-sized material from post-HCl leach sediment appear to show the unintended dissolution of smectite (Fig. 6). A shift of  $0.1^{\circ}$  20 was found between the 001 smectite position for the untreated and acetic acid treated samples. HCl had a greater effect on the smectites, shifting the 001 peak by  $0.5^{\circ}$  20 from the untreated sample. These shifts in the peak position may result from cation exchange, mineral dissolution, or both. Leached cations, such as  $Ca^{2+}$  or  $H^+$ , can exchange for  $K^+$  in the clay

interlayers, causing the interlayer inter-atomic spacing (d) to become smaller and  $2\theta$  to increase (Chipera et al., 1995). The untreated peak is broader toward higher  $2\theta$  values (Fig. 6), suggesting some of the smectite may be interstratified with illite (Drits et al., 1998). The XRD patterns for the HCl-treated smectites become even more asymmetrical. The dissolution of pure smectite would make the interstratified illite-smectite signal more prominent, explaining both the peak shift and the asymmetrical broadening. Therefore, some smectite-bound  $^{10}$ Be released in the HCl extraction was likely artificially over-counted as oxyhydroxide-bound  $^{10}$ Be in method 1. In the initial method (0B-i), fine clays were also subjected to a NH<sub>2</sub>OH–HCl leach, resulting in almost total loss of fine clay bound Be to prior acid extractions (Fig. 5).

#### 4.3. Grain size experiments

The effects of grain size on  $^{10}$ Be distribution investigated through method 3 (Fig. 3) show the relative phase abundances differ substantially between processing methods (Fig. 5). With coarse clay particles properly separated from silt in method 3, 40–60% of  $^{10}$ Be is identified as clay bound, compared with only 10–12% in method 2. Oxyhydroxide and residual silt fractions had proportionately more  $^{10}$ Be in method 2 than in method 3, where coarser clay fractions that settled within 24 h were classified with silt and subject to the oxyhydroxide leach. Adsorbed  $^{10}$ Be was relatively comparable between all methods, although a larger variation was found between the samples from method 3.

Sample 0B, the control sample subject to all three methods and the initial trial, shows the effects that the different methods have on the ultimate <sup>10</sup>Be yield and the relative phase abundance within the sample (Fig. 7). This was manifested as a 27% increase in total <sup>10</sup>Be yield from

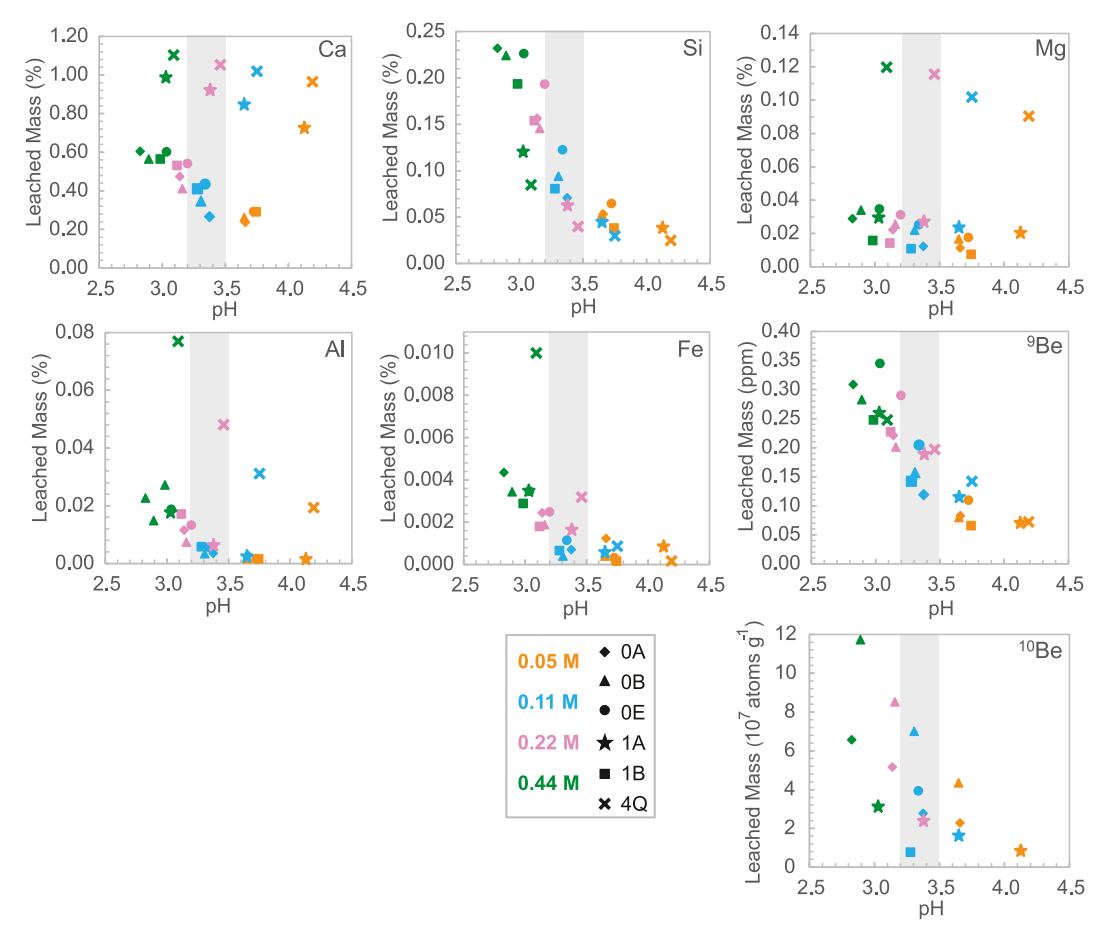
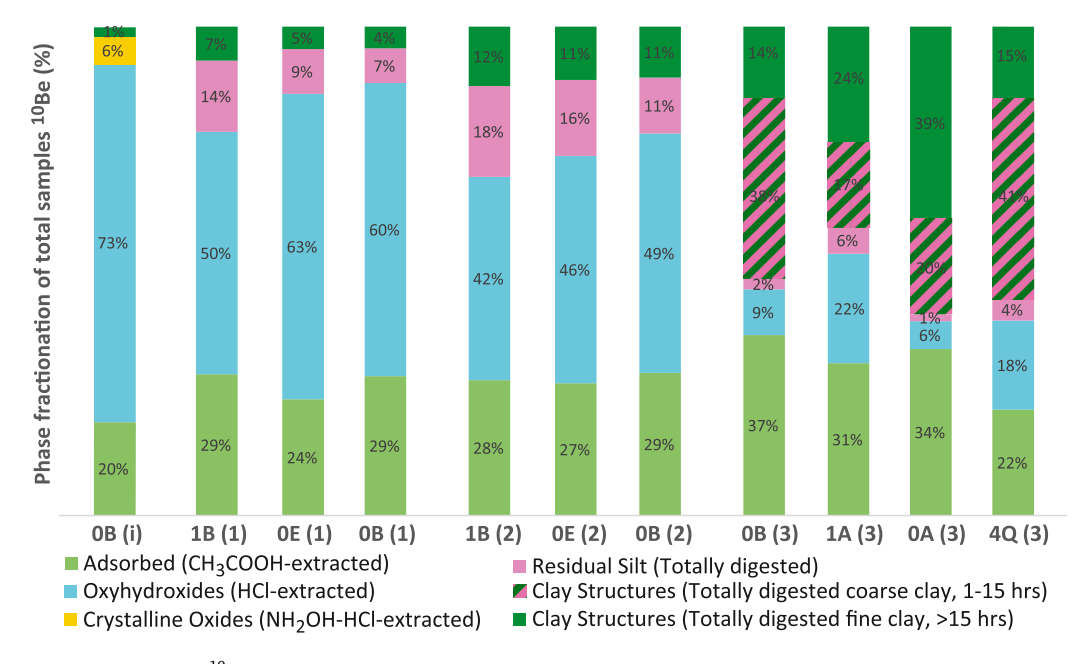
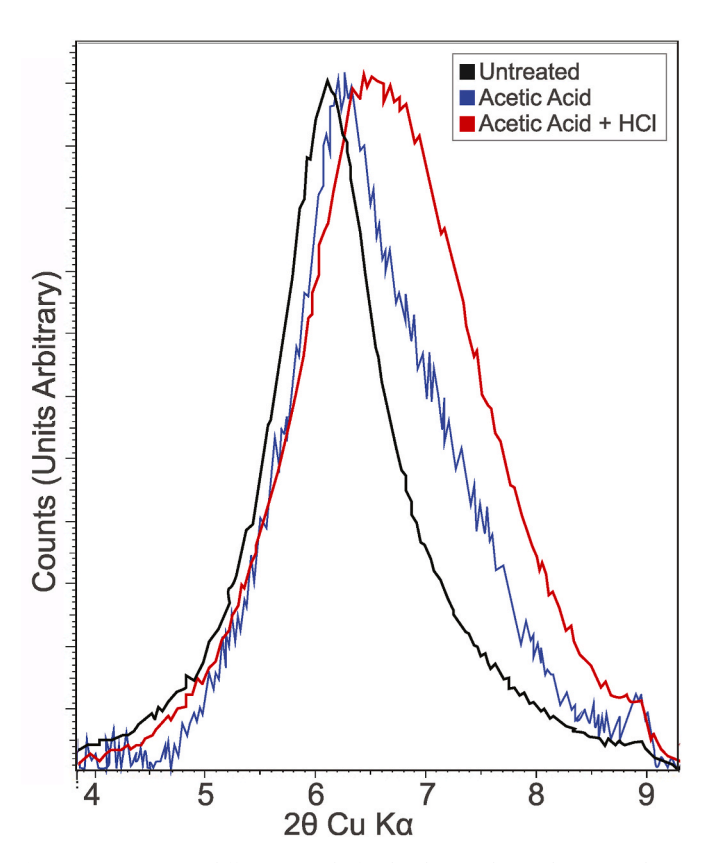


Fig. 4. Elemental yield as a function of pH at hour 4 of the acetic acid extractions, showing increased yield with decreased pH and the ideal range for maximum desorption of the elements without significantly affecting Si, Al, and Fe (shaded areas). The sample employed is shown by the symbol, the strength of acetic acid by the color.



**Fig. 5.** Relative phase distribution of total <sup>10</sup>Be concentrations of all samples. Methods are indicated in parentheses next to the sample name. In methods 1 and 2, the residual silt phases (pink) represent products settled over 24 h and is therefore equivalent to the residual silt and coarse clay structures from method 3. In method 3, the adsorbed phase is a sum product of the absorbed <sup>10</sup>Be concentration in silt, coarse clay, and fine clay and the fraction of those grain sizes in the total sample. The HCl-extracted fraction covers only silt in method 3, silt and coarse clay in method 2, and the entire sample in method 1.



**Fig. 6.** Smectite X-ray diffraction peaks for the clay sized particles in sample 0B show the effects of 0.11 M acetic acid (blue,  $2\theta = 6.2^{\circ}$ ) and 0.5 M HCl (red,  $2\theta = 6.6^{\circ}$ ). Black peak represents untreated sample ( $2\theta = 6.1^{\circ}$ ). All peaks rescaled for peak comparison. All other samples showed similar trends.

method 3 relative to methods 1 and 2 (Fig. 7a). Compared with method 2, method 3 saw the total  $^{10}$ Be in the adsorbed fraction increase by 60%, and a 70% increase in fine clay residual; the sum of the oxyhydroxide-

bound (HCl-extracted), coarse clay residual and silt residual <sup>10</sup>Be is nearly identical between the two methods (Fig. 7a). The initial trial (0B-i), in which the samples were dry sieved without a sonicator preparation, had even less absorbed <sup>10</sup>Be. Such difference in total beryllium concentrations from the same sample after similar extraction and digestion methods suggests that the initial sample preparation played a significant role in the process, most notably with the increased inclusion of clay-sized particles.

When the samples were vigorously disaggregated, partition of <sup>10</sup>Be between adsorbed, oxyhydroxide, residual and clay sediment fractions shows that clays were the primary host of <sup>10</sup>Be in the sediments (Fig. 8). Clay-bound <sup>10</sup>Be was highest in sample 0A at 60% of the total <sup>10</sup>Be, whereas it was lowest in sample 1A at 41% of the total sample <sup>10</sup>Be. The second most <sup>10</sup>Be-rich fraction in the freshly emerging samples is the adsorbed, at 22–37% of the total sample <sup>10</sup>Be. The oxyhydroxide-bound <sup>10</sup>Be content varied between 6% and 22%. Residual <sup>10</sup>Be was consistently the smallest fraction in all samples.

Meteoric <sup>10</sup>Be concentrations in the freshly emerging sediments at the Mt. Achernar Moraine were dependent on grain size, i.e. the smaller the grains, the higher the <sup>10</sup>Be concentrations. Clay and silt-sized particles contained 89–95% of the total <sup>10</sup>Be in the samples. Clays were the most <sup>10</sup>Be-rich size fraction in all cases, at 53–84%. The relative size difference between coarse clay (settled in 15 h) and fine clay (still in suspension after 15 h) did not appear to have a strong role in controlling <sup>10</sup>Be distribution, and the relative importance of the two fractions varied from sample to sample (Fig. 8). Of the clay-sized particles, clay minerals were the primary host of <sup>10</sup>Be over the adsorbed fraction. The adsorbed fraction is the dominant <sup>10</sup>Be fraction of the non-clay sized particles in samples 0A and 0B. In samples 1B and 4Q, the <sup>10</sup>Be in the non-clay sized particles was dominantly HCl-extractable <sup>10</sup>Be (Fig. 8).

## 4.4. 10Be/9Be ratio

In samples processed by method 3, 58–74% of total <sup>9</sup>Be is found in the clay phase (Appendix B). Methods 1 and 2 suggest only 20–29% of <sup>9</sup>Be fractionated into clay, with significantly higher yields in the oxyhydroxide and residual phases. In the freshly emerging samples, the

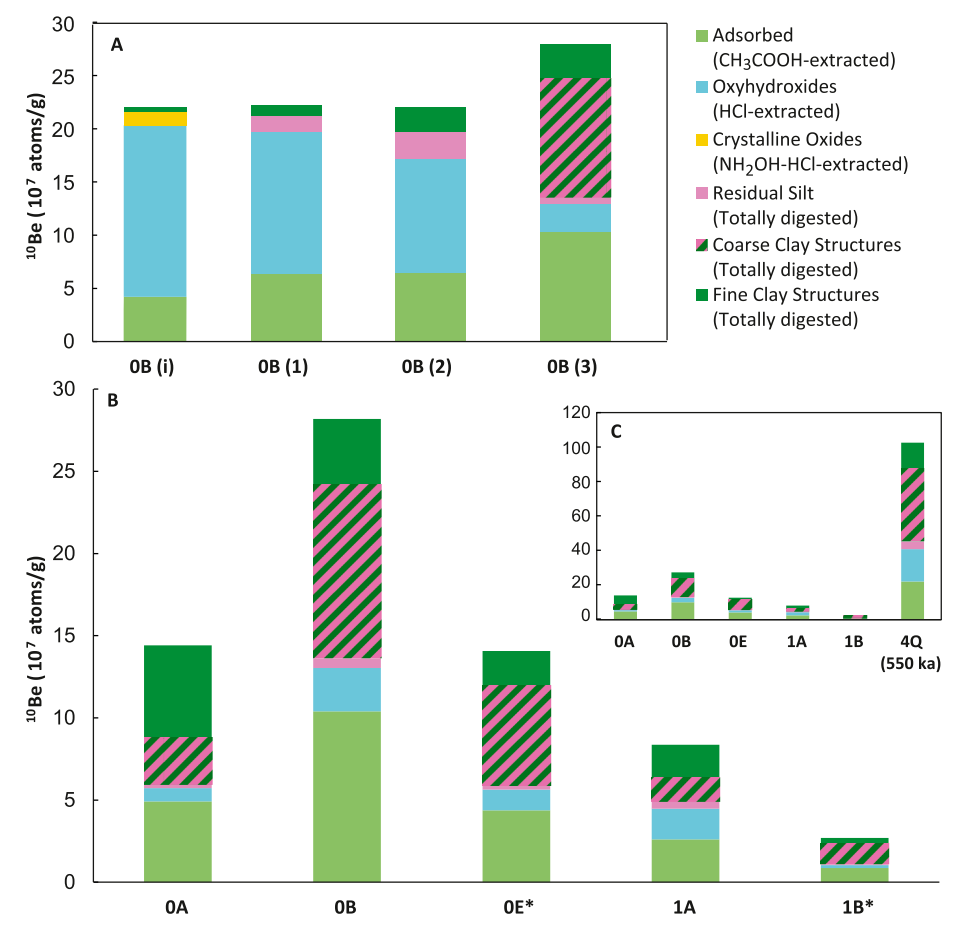


Fig. 7. Total <sup>10</sup>Be in each sample divided into the fraction in which it was measured. Panel A compares the run of sample 0B across all three methods and the initial trial method. All samples run by method 3 are compared in panel B. Panel C is an inset of B with the 550 ka surface-exposed sample (4Q) included. Total values for each fraction are calculated by weighting the average of each fraction in silt, coarse clay, and fine clay to the abundance of that grain size (data from fine sand-sized aliquots are not included). The asterisk-marked samples (OE and 1B) were not analyzed by method 3. Here the method 3 result is estimated from the average of methods 1 and 2. For each fraction (i.e. adsorbed, etc.) we multiply the ratio found between methods in sample 0B (Panel A) by the concentration of <sup>10</sup>Be within this fraction in 0E and 1B.

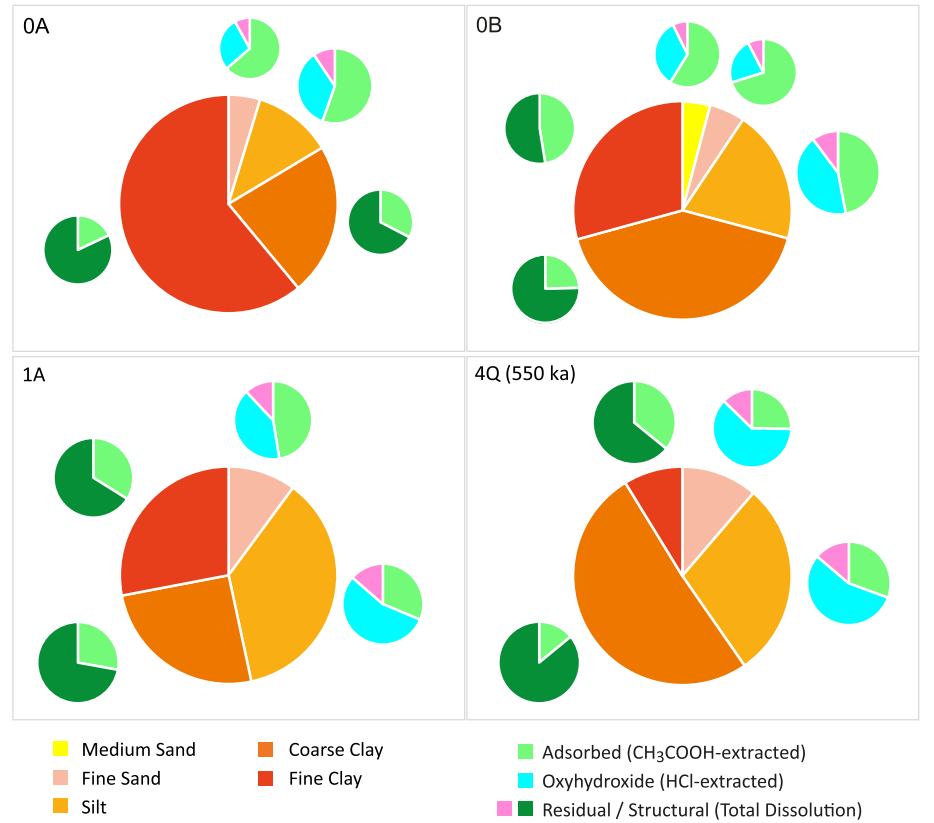


Fig. 8. Meteoric <sup>10</sup>Be concentrations in freshly emerging subglacial sediments (0A, 0B and 1A) are grain-size dependent, i.e. more <sup>10</sup>Be accumulates in smaller grain sizes than in larger grain sizes (larger, orange pie charts). Phase distribution of <sup>10</sup>Be (smaller pie charts) in the residual grain sizes (medium sand, fine sand, and silt) varies, with adsorbed species being the dominant <sup>10</sup>Be phase in samples 0A and 0B and oxyhydroxides more dominant in the calcite-rich sample 1A and the sample with a 550 ka exposure history, 4Q. In the clay-sized fraction, clay minerals are the dominant <sup>10</sup>Be hosts over adsorbed species in all cases. <sup>10</sup>Be was only measured in the medium sand fraction in sample 0B.

total  $^{10}$ Be/ $^{9}$ Be ratio ranges from 0.02 to 0.35·10 $^{-8}$ , depending on the  $^{10}$ Be content of the sample; the long-exposed sample (4Q) is  $0.69 \cdot 10^{-8}$ . These ratios are comparable to those found in Antarctic diamictites recovered from subglacial and marine settings (White et al., 2019; Yokoyama et al., 2016). When examining separately leached fractions individually, the  $^{10}$ Be/ $^{9}$ Be ratio is 1.6–2.4 times higher in the adsorbed phase than in the sample as a whole. Clays extracted by method 3 have  $a^{10}$ Be/ $^{9}$ Be ratio 0.7–0.8 that of the entire sample. This results in separate trends for each fraction when the  $^{10}$ Be/ $^{9}$ Be ratio is considered as function of meteoric  $^{10}$ Be concentration (Fig. 9).

## 4.5. Chemical controls on <sup>10</sup>Be distribution

Ca was the most abundant element in the acetic acid leach, suggesting calcium carbonate dissolution (Appendix B). Other elements were leached in only minor amounts in most samples. The yield did not differ significantly between methods 1 & 2 and the acetic acid leach at 0.11 M. However, method 3 produced greater yields of all elements, but especially for Al, Fe, and Si, which had 2-4 times greater yields (Appendix B). This suggests that the greater sample disaggregation increased the surface area for carbonate dissolution and cation exchange. Sample 4Q leached Fe, Al, and exchangeable ions in higher quantities than the freshly emerging samples (Appendix B).

The 0.5 M HCl extraction targeting oxyhydroxides yielded substantial quantities of Fe, Al, Si, Ca, and Mg (Appendix B). In method 1, Fe, Al, Si, and Ca each yielded 0.4–0.8% of sample mass; Mg ranged from 0.1 to 0.2% sample mass. Between methods 1 and 2, yields were 19–27% higher for all elements from method 1, where the clays were separated after the HCl extraction. The reduction in yield in method 2 was uniform across the major elements (Appendix B). In sample 0 B, where all three methods were tested, method 3 yielded only  $\sim\!\!35\%$  of the material of method 1, with the largest reductions in Mg and Ca (Appendix B). Sample 1A, which was calcite-rich, yielded substantially more material than the other samples on which method 3 was tested.

Total dissolution of the clay and residual samples was not always completely successful, with some fraction of residue withstanding total digestion. For the clay fraction, Al yields ranged between 11.4 and

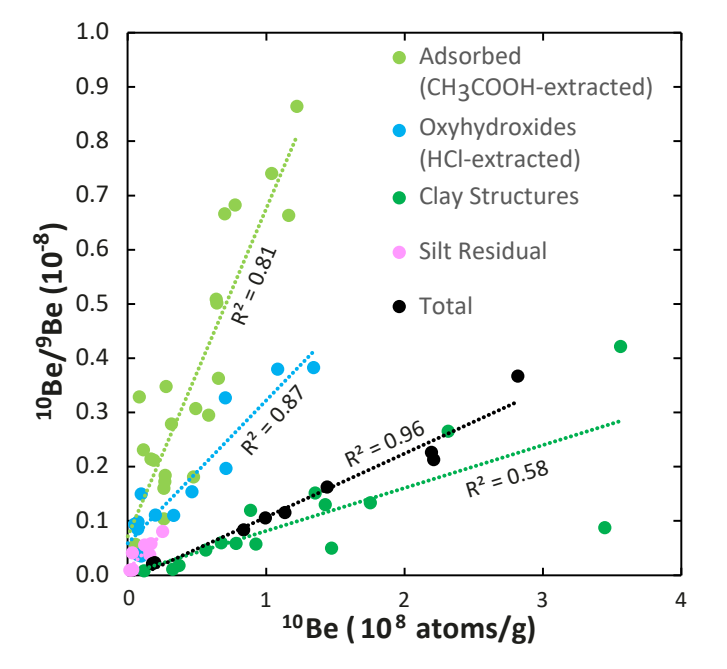


**Fig. 9.** The ratio of  $^{10}$ Be to  $^{9}$ Be vs  $^{10}$ Be concentration. Clay species have far lower ratios, suggesting substantial incorporation of lithogenic Be relative to grain-coating species. This may be explained by the mix of authigenic and detrital clay in the clay fraction.

15.4% in samples where total dissolution was successful; Fe ranged 5.4–6.5%. In the freshly emerging samples, fine clay was consistently enriched in Fe compared with coarse clay, and method 2 had higher Fe yields than method 1 (Appendix B).

#### 5. Discussion

#### 5.1. pH dependency of element adsorption/desorption

If the acetic acid extraction in our procedure is to quantify  $^{10}\mathrm{Be}$  adsorbed on the surface of mineral grains, yield of adsorbed elements must be maximized, especially  $^{10}\mathrm{Be}$ , while other beryllium-bearing grain components, such as oxides, oxyhydroxides, and clay minerals must be minimally affected. Acetic acid extractions both dissolve carbonates and desorb adsorbed species. Therefore, Ca and Mg released into solution could not be used as indicators for the dissolution of undesired phases due to their expected dissolution from carbonates. Si, Al, and Fe are indicators for the undesired dissolution of grain coatings and clays.

Stabilization of sample solution pH after 4 h (Appendix A) of leaching suggests that cation exchange between the acid and the samples was exhausted in approximately that time. All sample solution pH measurements were in the range where beryllium exists in solution and increasingly, exponentially, adsorbs to fine particles with increased pH (You et al., 1989). <sup>10</sup>Be data from the three samples subjected to the pH experiments agree with previously established desorption curves, showing increased yield/desorption of <sup>10</sup>Be with decreased pH (Fig. 4).

For the purposes of this study, a concentration of 0.11 M acetic acid is ideal to achieve maximal desorption of <sup>10</sup>Be and other adsorbed species while minimally affecting amorphous grain components and aluminosilicates. The 0.11 M sample solutions remained at a pH that yielded significantly more <sup>10</sup>Be than the 0.05 M solution and did not reach the pH 3.2 threshold at which Si, Al, and Fe yield significantly increases (Fig. 4). Soluble Fe and Al are commonly bound in oxides or oxyhydroxides (Drever, 1997; Stumm et al., 1996). Al<sup>3+</sup> can exist as a mobile cation in acidic (pH 3-4) environments, but its abundance as a free ion - not bound to ligand complexes, available for adsorption in natural systems is vanishingly small due to its high charge-to-radius ratio (Harris et al., 1996; Rumble, 2020). Graly et al. (2020) reported a decline in magnetic susceptibility in the moraine sediments relative to the source rock, indicating oxidizing conditions in the Mt. Achernar subglacial system. Soluble Fe<sup>2+</sup> is therefore unlikely to be abundant in the system. Al and Fe detected in the leachates indicate the undesired dissolution of more immobile phases, e.g. amorphous oxides or aluminosilicates, at pH < 3.2.

 $0.11\,M$  acetic acid is a standard concentration used for desorption in a variety of sequential extraction methods (Ure and Davidson, 2007), but this work suggests that pH monitoring during extraction is also needed, with more acid added in carbonate-rich conditions to assure complete desorption of Be from mineral surfaces. CaCO3 content in the samples is a potential contributing factor to adsorbed  $^{10}\text{Be}$  yield, preventing the desorption of  $^{10}\text{Be}$  (and other adsorbed species) by consuming the majority of the H+ ions available for exchange from the acid. In that case, CaCO3-rich samples might need higher concentrations of acetic acid to ensure that the pH stays within the 3.5–3.2 window in order to desorb all the available adsorbed  $^{10}\text{Be}$ . This effect can be seen on the calcite-rich samples, 1A and 4Q. All samples were measured over a small range of pH throughout the experiment, except 1A, which was always at significantly higher pH (Fig. 5).

## 5.2. Clay and grain size dependency of <sup>10</sup>Be distribution

The study of the effects of grain size on <sup>10</sup>Be distribution in the samples revealed that <sup>10</sup>Be concentrations in the samples were highly dependent on grain size (Fig. 8), consistent with previous studies (Boschi and Willenbring, 2021; Singleton et al., 2016; You et al., 1989) and

underscores the importance of clay minerals on <sup>10</sup>Be retention. There are two important differences between methods 2 and 3 that likely caused the differences in speciation and yield (Figs. 3, 5 and 7). First, the coarse clay fraction isolated by method 3 contains a significant portion of the  $^{10}$ Be counted as clay (Fig. 8). In methods 1 and 2, this was not counted as clay-bound 10Be and may be responsible for the significant residual and oxyhydroxide fractions in methods 1 and 2 (Fig. 5). Secondly, the vigorous disaggregation by mixing in a blender and sonication of the samples in method 3 before grain size separations and extractions meant that clay-sized particles encrusted onto larger silt and sand grains were not excluded during sieving or gravity separation. The  $\sim$ 27% greater <sup>10</sup>Be yield from method 3 (Fig. 7a) results from this process. Agglomeration of clay onto silt and sand also affected the relative phase distribution of <sup>10</sup>Be in the samples, making clays the dominant <sup>10</sup>Be host in method 3 as opposed to oxyhydroxides (HCl-extracted species) in methods 1 and 2 (Fig. 5). We interpret the relative dominance of oxyhydroxide phases in method 2 as representing the coarse clay fraction and finer clay particles that remained adhered to silt sized grains during separation. We cannot entirely rule out that oxyhydroxides are entering the clay fraction during sonication, however the proportions of K remain high in the clay fractions extracted by Method 3 (Appendix B), suggesting primarily clay mineral dissolution. Method 3 is therefore most likely to accurately represent the distribution of  ${}^{10}\mathrm{Be}$  between the sample phases. Likewise, vigorous grain disaggregation and analysis of coarser clay fractions may be appropriate to studies in other settings where grain coatings strongly adhere clays to larger particles.

For the samples included in method 3, the majority of the  $^{10}\mathrm{Be}$  in the clay-sized fractions comes from the total dissolution of the clay minerals, i.e. from within the clay mineral structures, as opposed to being adsorbed to the clay surfaces (Fig. 8). This holds true for the freshly emerging sediments as well as for sample 4Q, which likely received most of its <sup>10</sup>Be content from post-glacial deposition. In the larger grain sizes (silt, fine sand, and medium sand), the phase distribution differs between the calcite-rich samples (1A and 4Q), and the other freshly emerging sediments (Fig. 8). Adsorbed 10Be was most abundant, followed by HClextracted <sup>10</sup>Be (oxyhydroxides), in samples 0A and 0B, whereas the order was reversed in 1A and 4Q (Fig. 8). The potential cause for this effect may be the buffering of the acetic acid extraction by CaCO<sub>3</sub> (Fig. 4). In the case of the carbonate-rich samples, in which the pH level was higher, some adsorbed species seemed to withstand the acetic acid extraction and were leached into solution in the HCl extraction instead. Therefore, some of the 10Be in the oxyhydroxide (HCl-extracted) and clay fractions in samples 1A and 4Q might be adsorbed <sup>10</sup>Be.

## 5.3. Chemical and mineralogical controls on <sup>10</sup>Be distribution

Beryllium is known to adsorb to the surfaces of fine-grained sediment particles in aqueous systems, to precipitate with amorphous material, in particular HCl-extractable grain coatings, and be incorporated into clay minerals during chemical weathering (Barg et al., 1997; McHargue and Damon, 1991; Singleton et al., 2016). At Mt. Achernar Moraine, clays and amorphous, non-crystalline materials made up about half of the <63  $\mu$ m fraction of the sediments by weight, suggesting an array of potential  $^{10}$ Be hosts in the samples (Graly et al., 2020, 2022). The mineral and chemical properties of the samples can provide insight into the effects of the chemical procedures to which the samples are subject, and to determine the mineralogical characteristics that control  $^{10}$ Be retention in the sediments.

Acetic acid extractions were used to dissolve carbonates and adsorbed species in the samples due to Be's adsorption behavior in aqueous solution. Mg and Ca are species associated with carbonates, which in the case of these samples would be calcite and dolomite, although some Mg and Ca is likely also adsorbed to grain surfaces. The base cations, Ca<sup>2+</sup>, Mg<sup>2+</sup>, Na<sup>+</sup> and K<sup>+</sup> were expected to be the main species desorbing in the acetic acid leach (Rayment and Higginson, 1992). However, the presence of Fe, Al, and additional Si indicates the unintended dissolution of

amorphous phases or clay particles in small quantities in the weak acid. The acetic acid leaches consistently removed  $\sim\!0.1$  wt % Si (Appendix B); with 40 ml extractant per gram sample, this could be explained simply through dissolution of amorphous Si (Lindsey, 1979). The higher yields of all elements from the samples by method 3 (Appendix B) is most likely due to the more vigorous disaggregation of the sample. Clay-sized particles play a major role in sediment adsorption due to their large surface areas and surface charge, which attract ions from solution (Velde, 2013). Samples in method 3 included more clay-sized particles and disaggregated particle surfaces, explaining higher yields of desorbed species.

Though Be can affiliate with a hydroxide-carbonate ion at very high partial pressures of  $CO_2$  (Bruno et al., 1987), Be is unable to form carbonate structures (Southon et al., 1987). Therefore, no  $^{10}$ Be is expected to be associated with the dissolution of those species. However, the presence of carbonates seems to have buffered the pH of the acetic acid, making it less effective in desorbing adsorbed species in calcite-rich samples. That might explain the presence of Mg and Ca in the HCl extraction, as carbonates that withstood the acetic acid extraction, e.g., dolomite. Other possible Mg and Ca sources are phosphates and zeolites (Graly et al., 2020).

Oxides and oxyhydroxides were the targeted phases in the HCl extraction, and Al and Fe were the main expected products of the leach. In soils, Fe and Al oxyhydroxides are often significant Be hosts (Graly et al., 2010; Jungers et al., 2009). However, in this setting, Si, Na, and K yield suggests dissolution of other phases. XRD patterns indicate the dissolution of clay minerals in method 1 (Fig. 6), but continued K and Na yield from the HCl extractions of methods 2 & 3 may suggest that clay minerals were not completely physically separated and continued to dissolve (Appendix B). The allophane, zeolite, and phosphate mineral content reported in Graly et al. (2020) are also potential sources of Si and Al in the HCl leach.

There is a strong correlation between total <sup>10</sup>Be concentration and smectite abundance in the freshly emerging samples (Fig. 10). This strongly suggests that authigenic smectites are effective scavengers of meteoric <sup>10</sup>Be in the subglacial environment at Mt Achernar Moraine. If the acetic acid leach successfully removed adsorbed or clay interlayer Be, then meteoric <sup>10</sup>Be must occupy tetrahedral positions within the clay structures in the samples. Smectites are 2:1 clay minerals, with two tetrahedral sheets for each octahedral sheet in their structure. Kaolinite also shows a positive, though not statistically significant correlation with total <sup>10</sup>Be concentration (Fig. 10). Kaolinite is a 1:1 clay with half the tetrahedral sites per unit cell. Thus smectite clays have, in theory, the capacity to carry larger quantities of <sup>10</sup>Be than kaolinite.

## 5.4. The 550 ka sample (4Q)

Sample 4Q reveals what happens to the <sup>10</sup>Be concentration and distribution within the moraine's sediment with long-term exposure under cold and dry surface conditions. The sediments from which sample 4Q was collected had largely similar source rocks as the freshly emerging samples (Bader et al., 2017). The most notable differences between sample 4Q and the freshly emerging sediments are higher total meteoric <sup>10</sup>Be concentrations (from surface exposure), higher quantities of carbonates measured as calcite and dolomite and by relatively high total Mg and Ca content (Graly et al., 2020, 2022), and a higher yield of <sup>10</sup>Be in HCl-extractable (oxyhydroxide) phases (Fig. 7). Despite the lower quantities of smectite in sample 4Q, the relative distribution of  $^{10}$ Be is similar in 4Q as in the freshly emerging sediments (Fig. 7). This indicates similar  $^{10}\mathrm{Be}$  behavior, i.e. phase distribution and retention within the samples, in the subglacial environment and at the moraine surface. This result strongly implies authigenic clay formation continues on the moraine surface, confirming mass balance calculations (Graly et al., 2022).

Rough estimation of the expected  $^{10}$ Be inventory of sample 4Q after 550 ka on the moraine surface was made using the equation:

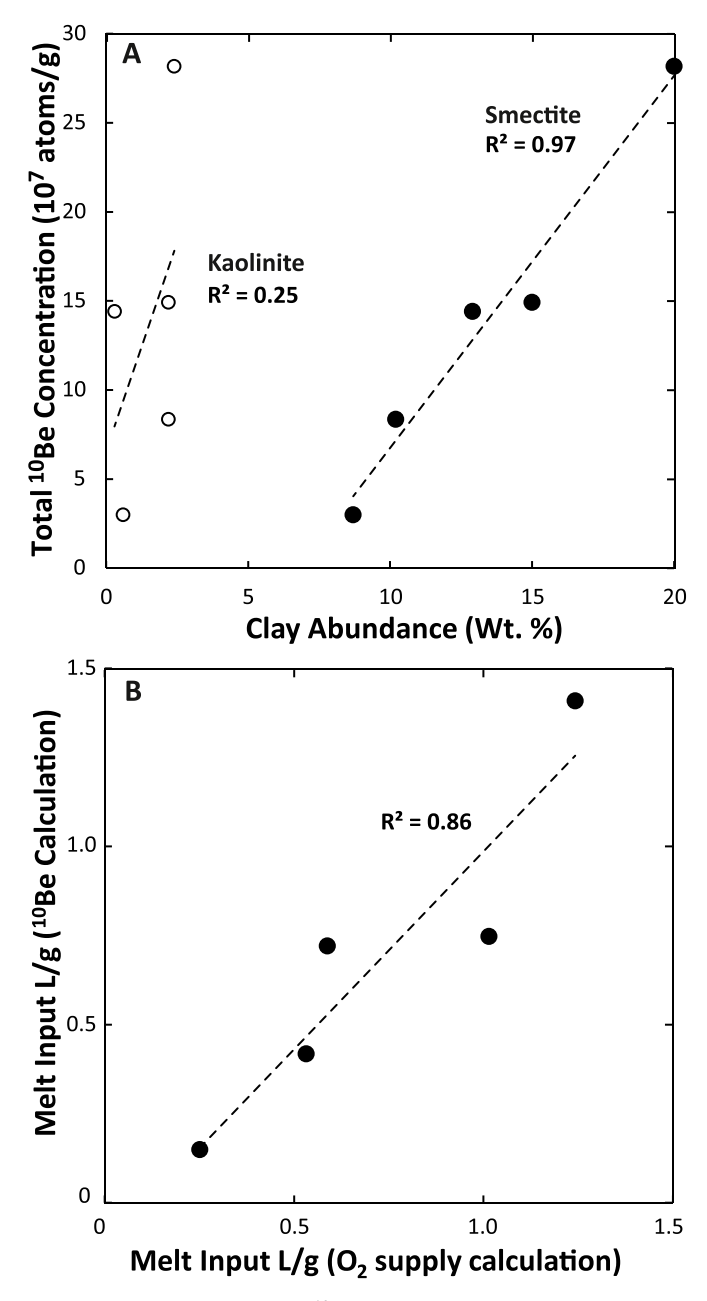


**Fig. 10.** Comparison of meteoric <sup>10</sup>Be inputs with chemical weathering products. A) Smectite and kaolinite concentrations (Graly et al., 2020) vs total meteoric <sup>10</sup>Be concentrations. B) Meltwater input per g sediment modeled from the excess smectite, kaolinite, calcite, and zeolites in samples compared with rock (Graly et al., 2020) vs meltwater input calculated from meteoric <sup>10</sup>Be concentration.

$$N = q(1 - e^{-\lambda t}) / \lambda \tag{1}$$

based on a surface meteoric  $^{10}$ Be deposition rate (q) of  $1.3\cdot10^5$  atoms·cm $^{-2}\cdot a^{-1}$  (Diaz et al., 2021; Steig et al., 1995) and the disintegration constant of meteoric  $^{10}$ Be,  $5.0\cdot10^{-7}$  a $^{-1}$  (Korschinek et al., 2010). According to these estimations, the inventory at the sample location is  $\sim 6.25\cdot10^{10}$  atoms cm $^{-2}$ . To convert our measurements to a total  $^{10}$ Be concentration, we need to estimate  $^{10}$ Be abundance in the grain sizes larger than fine sand, which were not measured at this location. Estimating the  $^{10}$ Be concentration in medium sand by assuming the same relative distribution of the isotope by grain size found in sample 0B, the total meteoric  $^{10}$ Be in grain sizes medium sand and below is  $6.14\cdot10^8$  atoms·g $^{-1}$ ; if particles coarse sand and above are

assumed to have no meteoric  $^{10}$ Be, the concentration is  $4.63\cdot10^8$  atoms·g $^{-1}$ . Taking these as a minimum and a maximum, this implies the meteoric  $^{10}$ Be inventory is spread over  $102-135~\rm g\cdot cm^{-2}$  of sediment, if our sample is typical. Assuming a till density of  $1.8~\rm g\cdot cm^{-3}$  (Graly et al., 2018b), a uniform meteoric  $^{10}$ Be profile would extend to  $57-75~\rm cm$  depth. Several locations in the Dry Valleys and Shackleton Glacier area have meteoric  $^{10}$ Be profiles where high concentrations extend to several  $10s~\rm of~cm$  of depth (Diaz et al., 2021; Schiller et al., 2009, 2014). Other meteoric  $^{10}$ Be profiles from the dry valleys show steep declines in meteoric  $^{10}$ Be concentration at depth (Dickinson et al., 2012; Graham et al., 2002; Valletta et al., 2015). This analysis suggests the former sort of profile is present here.

In situ  $^{10}$ Be is only a minor contributing factor in the residual fraction (totally digested quartz minerals) of sample 4Q. In situ concentrations in a corresponding boulder sample were on the order of  $10^6$  atoms·  $g_{quartz}^{-1}$  (Kaplan et al., 2017). Measured concentrations in the residual fraction of sample 4Q were  $4.12 \cdot 10^7$  atoms·  $g^{-1}$ , or one order of magnitude greater than should be expected for *in situ*  $^{10}$ Be in the fraction.

## 5.5. Subglacial weathering in the catchment of Law Glacier

Given the high partition coefficient of Be on solid surfaces (You et al., 1989) and the long residence times of the subglacial waters at the site, we can assume nearly 100% scavenging of the isotope onto solid material and consider the measured <sup>10</sup>Be concentrations in sediments to indicate the relative ratio of meltwater and till in the subglacial system. The accumulation of <sup>10</sup>Be in subglacial till is meltwater dependent, and the strong correlation between <sup>10</sup>Be and smectite abundances indicates that chemical weathering is governed by the input of ice melt and the oxygen therein. Two plausible reactants formed by oxidation reactions in the system could be responsible for the formation of secondary minerals due to dissolution of primary minerals in the source rock. Dissolution could take place due to carbonic acid, produced by the oxidation of organic matter from the rock of Beacon Supergroup, and due to sulfuric acid, produced by the oxidation of sulfides. Mass balance estimates in Graly et al. (2020) suggest that carbonic acid abundance in the system is at least an order magnitude larger than that of sulfuric acid, which is limited by sulfur abundance in the source rock. A likely weathering scenario for the samples begins with the subglacial dissolution of feldspars and pyroxenes by carbonic and/or sulfuric acid as oxygen was introduced to the system with meltwater. Meteoric <sup>10</sup>Be in the meltwater would adsorb to the surfaces of subglacial sediment particles but would take tetrahedral positions within smectite structures as authigenic clay formation occurs (Fig. 1).

Though we do not know the concentration of  $^{10}$ Be in the ice supplying Mt Achernar Moraine precisely, it is Pleistocene age (Graly et al., 2018c) and likely to be close to the  $^{10}$ Be concentration in ice of  $2 \cdot 10^5$  atoms·g $^{-1}$  found in the Vostok core (Raisbeck et al., 1992). Dividing the  $^{10}$ Be concentration of a sample by this assumed concentration in ice, we estimate meltwater input per g of <63  $\mu$ m material at the Mt. Achernar Moraine margin ranging from 150 ml for the sample with the least meteoric  $^{10}$ Be (1B) to 1400 ml for the most meteoric  $^{10}$ Be-enriched sample (0B). These values compare quite closely with those calculated by mass balance of the  $O_2$  necessary to form the carbonic and sulfuric acid required to produce the chemical weathering products in subglacial sediments (Fig. 10B) (Graly et al., 2020). We consider meteoric  $^{10}$ Be to provide a more accurate estimate of meltwater input, as it is not dependent on inferences about average bedrock composition.

The meltwater balance calculations provide two striking results describing local conditions at Mt. Achernar Moraine: the strong, direct dependence of smectite formation on meltwater input, and the heterogeneity of these meltwater inputs over relatively small spatial scales. The meltwater input calculation can be converted to a residence time of sediment in the subglacial environment only if the thickness of the actively weathering subglacial till is known. Based on a melt rate of 7.5 mm a $^{-1}$  (Pattyn, 2010), the residence time ranges from 140 to 1600

years per g <63  $\mu m$  sediment. Depending on till thickness, the true residence time could be 1 or 2 orders of magnitude higher. Some of the heterogeneity in meteoric  $^{10}\text{Be}$  meltwater input could reflect heterogeneity in the thickness of the underlying till or position within a weathering till profile prior to entrainment or a mix of entrainment locations between areas of greater and lesser weathering intensity.

The circumstances of the system described here, in which meteoric  $^{10}\mbox{Be}$  is shown to be a useful tracer for subglacial weathering processes, prevail on a larger scale across the continent. Given the widespread nature of the source rocks throughout the Transantarctic Mountains (Elliot et al., 2017; Isbell, 1990) and similar basal melting conditions (Pattyn, 2010) across the East Antarctic Ice Sheet, the processes that take place at the Mt. Achernar Moraine are likely to be representative of large portions of the continent. Using the approach presented here, meteoric <sup>10</sup>Be could potentially be used to infer subglacial chemical processes on a continent-scale in Antarctica. In order to apply this approach elsewhere in Antarctica, several important conditions need to be met. First, the glaciation history of the location should be considered in order to assess whether <sup>10</sup>Be could have been inherited from the source rock. Ideally, the area should have been ice-covered for many <sup>10</sup>Be half-lives, with no interglacial exposure. Second, the samples collected from blue ice moraines should have had minimal exposure on the surface. Therefore, freshly emerging sediments still in contact with/embedded in the ice are preferable. Third, formation of authigenic minerals may be dependent on the subglacial geology containing oxidizable material such as sulfides or organic carbon needed for the formation of carbonic and/or sulfuric acid, which are responsible for the dissolution of the source rock. Therefore, there may be regions of Antarctica outside the Transantarctic Mountains were oxygen input from meltwater is not the limiting factor on subglacial chemical weathering. The speciation of meteoric <sup>10</sup>Be between adsorption and various weathering products has the potential to distinguish between these settings.

#### 6. Conclusions

A sequential chemical extraction procedure was designed and adjusted to optimize the quantification of meteoric  $^{10}\mathrm{Be}$  content in weathering products from subglacially derived sediments at a blue ice moraine in the central Transantarctic Mountains. This study shows that vigorous disaggregation prior to grain size separation and chemical extractions is an important factor for the accurate quantification of <sup>10</sup>Be speciation in the till samples. 10Be bound within the structures of authigenic smectite is the dominant fraction of the nuclide in the samples and thus it is important to ensure that fine-grained particles are not unintentionally sieved out during initial sample preparation due to agglomeration to larger grains. For the desorption of adsorbed species, the pH level of the extractant should be maintained above 3.2 to avoid undesired dissolution of more immobile species, and below 3.5 to desorb the maximum amount of  $^{10}\mathrm{Be}$ . This customizing of the  $^{10}\mathrm{Be}$  extraction procedure for the solubility of the weathering products particular to individual samples may be broadly applied in other settings where <sup>10</sup>Be distribution among mineral species are considered.

Meteoric  $^{10}$ Be concentrations of 2–28·10 $^7$  atoms·g $^{-1}$  in abundant weathering products in freshly emerging subglacial sediments strongly indicate chemical weathering in the subglacial environment of the Mt. Achernar Moraine catchment area. In the area, which has been ice covered for >30 Ma years, meteoric  $^{10}$ Be is supplied to the subglacial sediments via subglacial meltwater. Oxyhydroxides and clay minerals host 64–70% of the total  $^{10}$ Be in the samples, indicating sufficient water and oxygen supply to perform chemical weathering which results in the formation of secondary minerals and amorphous weathering products. Strong correlation of smectite with  $^{10}$ Be content (R = 0.97) in the samples suggests that authigenic smectite formation takes place in the subglacial environment.

The weathering processes described in this study can potentially be extrapolated to continent-scale weathering rates by examining

subglacially derived sediments from across the continent using meteoric <sup>10</sup>Be as a tracer. This study introduces an approach with the potential to estimate Antarctica's contribution to global geochemical cycles via subglacial chemical weathering.

## Declaration of competing interest

The authors declare that they have no known competing financial interests or personal relationships that could have appeared to influence the work reported in this paper.

### Data availability

The data that underly this work are in the supplementary appendix.

#### Acknowledgments

The work was made possible by funding from National Science Foundation grant PLR-1744879. B. Geohring, G. Chmiel, H. Johnston, C. Watkins, and Hamna assisted with laboratory analyses. The US Antarctic Program, Kenn Borek Air, Ltd., and field team members from the 2010 and 2015 seasons are gratefully acknowledged for their role in sample collection. We would like to acknowledge the Integrated Nanosystems Development Institute (INDI) for use of their Bruker D8 Discover X-Ray Diffraction Instrument, which was awarded through NSF grant MRI-1429241. Editing by Pierre-Henri Blard and two careful, insightful reviews led to several improvements to the manuscript.

#### Supplementary data

Supplementary data to this article can be found online at https://doi.org/10.1016/j.quageo.2023.101458.

## References

- Anderson, S.P., 2005. Glaciers show direct linkage between erosion rate and chemical weathering fluxes. Geomorphology 67, 147–157.
- Bader, N.A., Licht, K.J., Kaplan, M.R., Kassab, C., Winckler, G., 2017. East Antarctic ice sheet stability recorded in a high-elevation ice-cored moraine. Quat. Sci. Rev. 159, 88-102
- Barg, E., Lal, D., Pavich, M.J., Caffee, M.W., Southon, J.R., 1997. Beryllium geochemistry in soils; evaluation of <sup>10</sup>Be/<sup>9</sup>Be ratios in authigenic minerals as a basis for age models. Chem. Geol. 140, 237–258.
- Barrett, P., Hambrey, M., Christoffersen, P., Glasser, N., Hubbart, B., 2007. Cenozoic Climate and Sea Level History from Glacimarine Strata off the Victoria Land Coast, Cape Roberts Project, Antarctica, Glacial Sedimentary Processes and Products. International Association of Sedimentologists, pp. 259–287.
- Barrett, P.J., Elliot, D.H., Lindsay, J.F., 1986. The Beacon Supergroup (Devonian-Triassic) and ferrar group (jurrasic) in the beardmore Glacier area, Antarctica. Geology of the central Transantarctic Mountains 36, 339–428.
- Bernet, M., Gaupp, R., 2005. Diagenetic history of triassic sandstone from the Beacon Supergroup in central victoria land, Antarctica. N. Z. J. Geol. Geophys. 48, 447–458.
- Bernhardt, A., Oelze, M., Bouchez, J., von Blanckenburg, F., Mohtadi, M., Christl, M., Wittmann, H., 2020. 10Be/9Be ratios reveal marine authigenic clay formation. Geophys. Res. Lett. 47, e2019GL086061.
- Beus, A.A., 1956. Geochemistry of beryllium. Geochemistry (USSR) English Trans. 1, 511–531.
- Bintanja, R., 1999. On the glaciological, meteorological, and climatological significance of Antarctic blue ice areas. Rev. Geophys. 37, 337–359.
- Boschi, V., Willenbring, J., 2016. Beryllium Desorption from Minerals and Organic Ligands over Time.
- Boschi, V., Willenbring, J.K., 2021. Chemical and physical drivers of beryllium retention in two soil endmembers. Sci. Total Environ. 754, 141591.
- Bruno, J., Grenthe, I., Muñoz, M., 1987. Studies of metal carbonate equilibria. Part 16.

  The beryllium (II)–water–carbon dioxide (g) system in neutral-to-alkaline 3.0 mol dm–3 perchlorate media at 25° C. J. Chem. Soc.. Dalton Trans. 2445–2449.
- Buchner, M.R., 2020. Beryllium coordination chemistry and its implications on the understanding of metal induced immune responses. Chem. Commun. 56, 8895–8907.
- Chipera, S.J., Carey, J.W., Bish, D.L., 1995. Controlled-humidity XRD analyses: application to the study of smectite expansion/contraction. Adv. X Ray Anal. 39, 713–722.
- Chipera, S.J., Guthrie Jr., G., Bish, D.L., 1993. Preparation and Purification of Mineral Dusts. Mineralogical Society of America, Washington, DC (United States).

- Corbett, L.B., Bierman, P.R., Neumann, T.A., Graly, J.A., Shakun, J.D., Goehring, B.M., Hidy, A.J., Caffee, M.W., 2021. Measuring multiple cosmogenic nuclides in glacial cobbles sheds light on Greenland Ice Sheet processes. Earth Planet Sci. Lett. 554, 116673
- DeConto, R.M., Pollard, D., 2003. A coupled climate-ice sheet modeling approach to the Early Cenozoic history of the Antarctic ice sheet. Palaeogeogr. Palaeoclimatol. Palaeoecol. 198. 39–52.
- Diaz, M.A., Corbett, L.B., Bierman, P.R., Adams, B.J., Wall, D.H., Hogg, I.D., Fierer, N., Lyons, W.B., 2021. Relationship between meteoric 10 Be and NO 3– concentrations in soils along Shackleton Glacier, Antarctica. Earth Surf. Dyn. 9, 1363–1380.
- Dickinson, W.W., Schiller, M., Ditchburn, B.G., Graham, I.J., Zondervan, A., 2012. Meteoric Be-10 from sirius group suggests high elevation McMurdo dry valleys permanently frozen since 6 Ma. Earth Planet Sci. Lett. 355, 13–19.
- Ditchburn, R., Whitehead, N., 1994. The Separation of <sup>10</sup>Be from Silicates. Proc. Third Workshop of the South Pacific Environmental Radioactivity Association, pp. 4–7.
- Drever, J.I., 1997. The Geochemistry of Natural Waters: Surface and Groundwater Environments. Prentice Hall.
- Drits, V.A., Eberl, D.D., Srodon, J., 1998. XRD measurement of mean thickness, thickness distribution and strain for illite and illite-smectite crystallites by the Bertaut-Warren-Averbach technique. Clay Clay Miner. 46, 38–50.
- Du Laing, G., 2011. Redox metal processes and controls in estuaries. In: Wolanski, E., McLusky, D. (Eds.), Treatise on Estuarine and Coastal Science. Academic Press, Waltham, pp. 115–141.
- Elliot, D.H., Fanning, C.M., Isbell, J.L., Hulett, S.R., 2017. The Permo-Triassic Gondwana sequence, central Transantarctic Mountains, Antarctica: zircon geochronology, provenance, and basin evolution. Geosphere 13, 155–178.
- Everest, D., Bailar, J., Emeléus, H., Nyholm, R., Trotman-Dickenson, A., 1973. Beryllium. Comprehensive inorganic chemistry 1, 531–590.
- Everest, D.A., 1964. The Chemistry of Beryllium. Elsevier Pub. Co.
- Filippelli, G.M., 2008. The global phosphorus cycle: past, present, and future. Elements 4, 89–95.
- Graham, I.J., Ditchburn, R.G., Claridge, G.G.C., Whitehead, N.E., Zondervan, A., Sheppard, D.S., 2002. Dating Antacrtic Soils Using Atmosphere-Derived <sup>10</sup>Be and Nitrate, vol. 35. Royal Society of New Zealand Bulletin, pp. 429–436.
- Graly, J.A., Bierman, P.R., Reusser, L.J., Pavich, M.J., 2010. Meteoric <sup>10</sup>Be in soil profiles
   a global meta-analysis. Geochem. Cosmochim. Acta 74, 6814–6829.
- Graly, J.A., Corbett, L.B., Bierman, P.R., Lini, A., Neumann, T.A., 2018a. Meteoric <sup>10</sup>Be as a tracer of subglacial processes and interglacial surface exposure in Greenland. Quat. Sci. Rev. 191, 118–131.
- Graly, J.A., Drever, J.I., Humphrey, N.F., 2017. Calculating the balance between atmospheric CO<sub>2</sub> drawdown and organic carbon oxidation in subglacial hydrochemical systems. Global Biogeochem. Cycles 31, 709–727.
- Graly, J.A., Licht, K.J., Bader, N.A., Bish, D.L., 2020. Chemical weathering signatures from Mt. Achernar Moraine, Central Transantarctic Mountains I: subglacial sediments compared to underlying rock. Geochem. Cosmochim. Acta 283, 149–166.
- Graly, J.A., Licht, K.J., Bader, N.A., Kassab, C.M., Bish, D.L., Kaplan, M.R., 2022.
  Chemical weathering signatures at Mt. Achernar, central transantarctic Mountains II: surface exposed sediments. Geochem. Cosmochim. Acta (Accepted).
- Graly, J.A., Licht, K.J., Druschel, G.K., Kaplan, M.R., 2018b. Polar desert chronologies through quantitative measurements of salt accumulation. Geology 46, 351–354.
- Graly, J.A., Licht, K.J., Kassab, C.M., Bird, B.W., Kaplan, M.R., 2018c. Warm-based basal sediment entrainment and far-field Pleistocene origin evidenced in central Transantarctic blue ice through stable isotopes and internal structures. J. Glaciol. 64, 185–196.
- Harris, W.R., Berthon, G., Day, J.P., Exley, C., Flaten, T.P., Forbes, W.F., Kiss, T., Orvig, C., Zatta, P.F., 1996. Speciation of aluminum in biological systems. J. Toxicol. Environ. Health, Part A 48, 543–568.
- Hawthorne, F.C., Huminicki, D.M., 2002. The crystal chemistry of beryllium. Rev. Mineral. Geochem. 50, 333–403.
- Isbell, J.L., 1990. Fluvial Sedimentology and Basin Analyses of the Permian Fairchild and Buckley Formations, Beardmore Glacier Region, and the Weller Coal Measures, Southern Victoria Land, Antarctica. The Ohio State University.
- Jamieson, S.S., Sugden, D.E., Hulton, N.R., 2010. The evolution of the subglacial landscape of Antarctica. Earth Planet Sci. Lett. 293, 1–27.
- Jungers, M.C., Bierman, P.R., Matmon, A., Nichols, K., Larsen, J., Finkel, R., 2009. Tracing hillslope sediment production and transport with in situ and meteoric  $^{10}$ Be 114.
- Kabata-Pendias, A., Pendias, H., 1984. Trace Elements in Soil and Plants. CRC Press, Inc. Kaplan, M., Licht, K.J., Winckler, G., Schaefer, J., Bader, N., Mathieson, C., Roberts, M., Kassab, C.M., Schwartz, R., Graly, J.A., 2017. Middle to late Pleistocene stability of the central East Antarctic ice sheet at the head of Law Glacier. Geology 45, 963–966.
- Kaplan, M.R., Licht, K.J., Lamp, J.L., Winckler, G., Schaefer, J.M., Graly, J.A., Kassab, C. M., Schwartz, R., 2022. Paleoglaciology of the central East Antarctic ice sheet as revealed by blue-ice sediment. Quat. Sci. Rev. (Accepted Manuscript).
- Kaplan, M.R., Strelin, J.A., Schaefer, J.M., Denton, G.H., Finkel, R.C., Schwartz, R., Putnam, A.E., Vandergoes, M.J., Goehring, B.M., Travis, S.G., 2011. In-situ cosmogenic <sup>10</sup>Be production rate at Lago Argentino, Patagonia: implications for lateglacial climate chronology. Earth Planet Sci. Lett. 309, 21–32.
- Kassab, C.M., Licht, K.J., Petersson, R., Lindbäck, K., Graly, J.A., Kaplan, M.R., 2020. Formation and evolution of an extensive blue ice moraine in central Transantarctic Mountains, Antarctica. J. Glaciol. 66, 49–60.
- Korschinek, G., Bergmaier, A., Faestermann, T., Gerstmann, U., Knie, K., Rugel, G., Wallner, A., Dillmann, I., Dollinger, G., Von Gostomski, Lierse, C., 2010. A new value for the half-life of 10Be by heavy-ion elastic recoil detection and liquid scintillation counting. Nucl. Instrum. Methods Phys. Res., Sect. B 268, 187–191.

- Kump, L.R., Brantley, S.L., Arthur, M.A., 2000. Chemical weathering, atmospheric CO<sub>2</sub> and climate. Annu. Rev. Earth Planet Sci. 28, 611–667.
- Li, X., Wang, N., Ding, Y., Hawkings, J.R., Yde, J.C., Raiswell, R., Liu, J., Zhang, S., Kang, S., Wang, R., 2022. Globally elevated chemical weathering rates beneath glaciers. Nat. Commun. 13, 1–13.
- Li, Y.-H., Burkhardt, L., Buchholtz, M., O'Hara, P., Santschi, P.H., 1984. Partition of radiotracers between suspended particles and seawater. Geochem. Cosmochim. Acta 48, 2011–2019.
- Lindsey, W.L., 1979. Chemical Equilibria in Soils.
- Lum, K.R., Gammon, K.L., 1985. Geochemical availability of some trace and major elements in surficial sediments of the Detroit River and western Lake Erie. J. Great Lake. Res. 11, 328–338.
- McHargue, L., Damon, P., 1991. The global beryllium 10 cycle. Rev. Geophys. 29, 141–158.
- Michaud, A.B., Skidmore, M.L., Mitchell, A.C., Vick-Majors, T.J., Barbante, C., Turetta, C., vanGelder, W., Priscu, J.C., 2016. Solute sources and geochemical processes in subglacial lake whillans, west Antarctica. Geology 44, 347–350.
- Morris, J., Valentine, R., Harrison, T., 2002. 10Be imaging of sediment accretion and subduction along the northeast Japan and Costa Rica convergent margins. Geology 30, 59–62.
- Nyffeler, U.P., Li, Y.-H., Santschi, P.H., 1984. A kinetic approach to describe traceelement distribution between particles and solution in natural aquatic systems. Geochem. Cosmochim. Acta 48, 1513–1522.
- Ochs, M., Ivy-Ochs, S., 1997. The chemical behavior of Be, Al, Fe, Ca and Mg during AMS target preparation from terrestrial silicates modeled with chemical speciation calculations. Nucl. Instrum. Methods Phys. Res. Sect. B Beam Interact. Mater. Atoms 123, 235–240.
- Palmer, E.F., Licht, K.J., Swope, R.J., Hemming, S.R., 2012. Nunatak Moraines as a Repository of what Lies beneath the East Antarctic Ice Sheet, vol. 487. Geological Society of America Special Paper, pp. 97–104.
- Pattyn, F., 2010. Antarctic subglacial conditions inferred from a hybrid ice sheet/ice stream model. Earth Planet Sci. Lett. 295, 451–461.
- Paxman, G.J., Jamieson, S.S., Hochmuth, K., Gohl, K., Bentley, M.J., Leitchenkov, G., Ferraccioli, F., 2019. Reconstructions of antarctic topography since the eocene–oligocene boundary. Palaeogeogr. Palaeoclimatol. Palaeoecol. 535, 109346.
- Petsch, S.T., 2014. Weathering of organic carbon. Treatise on Geochemistry 12 (Elsevier, ed. 2), 217–238.
- Pollard, D., DeConto, R.M., 2009. Modelling West Antarctic ice sheet growth and collapse through the past five million years. Nature 458, 329.
- Raisbeck, G.M., Yiou, F., Bourles, D., Lorius, C., Jouzel, J., Barkov, N.I., 1987. Evidence for two intervals of enhanced 10 Be deposition in Antarctic ice during the last glacial period. Letters to Nature 326, 273.
- Raisbeck, G.M., Yiou, F., Jouzel, J., Petit, J.R., 1990. <sup>10</sup>Be and  $\delta^2$ H in polar ice cores as a probe of the solar variability influence on climate. Philos. Trans. R. Soc. London, Ser. A 330, 463–470.
- Raisbeck, G.M., Yiou, F., Jouzel, J., Petit, J.R., Barkov, N.I., Bard, E., 1992. <sup>10</sup>Be deposition at Vostok, Antarctica during the last 50,000 years and its relationship to possible cosmogenic production variations during this period. In: Bard, E., Broecker, W.S. (Eds.), The Last Deglaciation: Absolute and Radiocarbon Chronologies. Springer-Verlag, Berlin, pp. 127–139.
- Raiswell, R., Canfield, D.E., 2012. The iron biogeochemical cycle past and present. Geochemical perspectives 1, 1–220.
- Rankama, K., Sahama, K., 1950. Th. G. Geochemistry.—Univ. Chicago Press (Chicago).
   Rayment, G., Higginson, F.R., 1992. Australian Laboratory Handbook of Soil and Water Chemical Methods. Inkata Press Pty Ltd.
- Relph, K.E., Stevenson, E.I., Turchyn, A.V., Antler, G., Bickle, M.J., Baronas, J.J., Darby, S.E., Parsons, D.R., Tipper, E.T., 2021. Partitioning riverine sulfate sources using oxygen and sulfur isotopes: implications for carbon budgets of large rivers. Earth Planet Sci. Lett. 567, 116957.
- Rumble, J., 2020. CRC Handbook of Chemistry and Physics, 101 ed. CRC Press.Ryan, J.G., 2002. Trace-element systematics of beryllium in terrestrial materials. Rev.Mineral. Geochem. 50, 121–145.
- Schiller, M., Dickinson, W., Ditchburn, R.G., Graham, I.J., Zondervan, A., 2009.
  Atmospheric <sup>10</sup>Be in an Antarctic soil: implications for climate change. J. Geophys. Res. 114, F01033.
- Schiller, M., Dickinson, W., Zondervan, A., Ditchburn, R., Wang, N., 2014. Rapid soil accumulation in a frozen landscape. Geology 42, 335–338.
- Shakun, J.D., Corbett, L.B., Bierman, P.R., Underwood, K., Rizzo, D.M., Zimmerman, S. R., Caffee, M.W., Naish, T., Golledge, N.R., Hay, C.C., 2018. Minimal East Antarctic Ice Sheet retreat onto land during the past eight million years. Nature 558, 284–287.
- Singleton, A., Schmidt, A., Bierman, P., Rood D, H., Neilson, B., T Sophie Greene, E., Bower J, A., Perdrial, N., 2016. Effects of grain size, mineralogy, and acidextractable grain coatings on the distribution of the fallout radionuclides 7Be 10Be, 137Cs and 210Pb in river sediment.
- Skidmore, M., Tranter, M., Tulaczyk, S., Lanoil, B., 2010. Hydrochemistry of ice stream beds - evaporitic or microbial effects? Hydrol. Process. 24, 517–523.
- Southon, J., Ku, T., Nelson, D., Reyss, J., Duplessy, J., Vogel, J., 1987. 10Be in a deep-sea core: implications regarding10Be production changes over the past 420 ka. Earth Planet Sci. Lett. 85, 356–364.
- Steig, E., Stuiver, M., Polissar, P., 1995. Cosmogenic isotope concentrations at taylor Dome, Antarctica. Antarct. J. U. S. 30, 95–97.
- Stumm, W., Morgan, J.J., Drever, J.I., 1996. Aquatic chemistry. J. Environ. Qual. 25, 1162.
- Takahashi, Y., Minai, Y., Ambe, S., Makide, Y., Ambe, F., 1998. Comparison of Adsorption Behavior of Multiple Inorganic Ions and Silica in the Presence of Humic Acid Using the Multitracer Technique.

- Tanner, C., Jackson, M., 1947. Nomographs of Sedimentation Times for Soil Particles under Gravity or Centrifugal Acceleration. Soil Science Society of America Proceedings, pp. 60–65.
- Tessier, A., Campbell, P.G.C., Bisson, M., 1979. Sequential extraction procedure for the speciation of particulate trace metals. Anal. Chem. 51, 844–851.
- Torres, M.A., Moosdorf, N., Hartmann, J., Adkins, J.F., West, A.J., 2017. Glacial weathering, sulfide oxidation, and global carbon cycle feedbacks. Proc. Natl. Acad. Sci. USA 114, 8716–8721.
- Tranter, M., Sharp, M.J., Lamb, H.R., Brown, G.H., Hubbard, B.P., Willis, I.C., 2002. Geochemical weathering at the bed of the Haut Glacier d'Arolla, Switzerland - a new model. Hydrol. Process. 16, 959–993.
- Ure, A., Davidson, C., 2007. Chemical speciation in soils and related materials by selective chemical extraction. In: Chemical Speciation in the Environment, second ed. Wiley-Blackwell, pp. 265–300.
- Valletta, R.D., Willenbring, J.K., Lewis, A.R., Ashworth, A.C., Caffee, M., 2015. Extreme decay of meteoric beryllium-10 as a proxy for persistent aridity. Sci. Rep. 5, 1–7.
- Velde, B., 2013. Origin and Mineralogy of Clays: Clays and the Environment. Springer Science & Business Media.
- Vesely, J., Norton, S.A., Skrivan, P., Majer, V., Kram, P., Navrátil, T., Kaste, J.M., 2018. Environmental chemistry of beryllium. In: Edward, S.G. (Ed.), Reviews in Mineralogy & Geochemistry: Beryllium Mineralogy, Petrology, and Geochemistry. De Gruyter, pp. 291–318.
- Wadham, J.L., Arndt, S., Tulaczyk, S., Stibal, M., Tranter, M., Telling, J., Lis, G., Lawson, E., Ridgwell, A., Dubnick, A., 2012. Potential methane reservoirs beneath Antarctica. Nature 488, 633–637.
- Wang, Q., Zhu, C., Yun, J., Yang, G., 2017. Isomorphic substitutions in clay materials and adsorption of metal ions onto external surfaces: a DFT investigation. J. Phys. Chem. C 121, 26722–26732.

- White, D.A., Fink, D., Post, A.L., Simon, K., Galton-Fenzi, B., Foster, S., Fujioka, T., Jeromson, M.R., Blaxell, M., Yokoyama, Y., 2019. Beryllium isotope signatures of ice shelves and sub-ice shelf circulation. Earth Planet Sci. Lett. 505, 86–95.
- Wiederhold, J.G., Teutsch, N., Kraemer, S.M., Halliday, A.N., Kretzschmar, R., 2007. Iron isotope fractionation in oxic soils by mineral weathering and podzolization. Geochem. Cosmochim. Acta 71, 5821–5833.
- Wilson, D.S., Jamieson, S.S., Barrett, P.J., Leitchenkov, G., Gohl, K., Larter, R.D., 2012. Antarctic topography at the eocene-oligocene boundary. Palaeogeogr. Palaeoclimatol. Palaeoecol. 335, 24–34.
- Wittmann, H., Blanckenburg, F., Bouchez, J., Dannhaus, N., Naumann, R., Christl, M., Gaillardet, J., 2012. The dependence of meteoric <sup>10</sup>Be concentrations on particle size in Amazon River bed sediment and the extraction of reactive <sup>10</sup>Be/<sup>9</sup>Be ratios. Chem. Geol. 318, 126–138.
- Yiou, F., Raisbeck, G., Bourles, D., Lorius, C., Barkov, N., 1985. 10Be in ice at Vostok Antarctica during the last climatic cycle. Nature 316, 616.
- Yokoyama, Y., Anderson, J.B., Yamane, M., Simkins, L.M., Miyairi, Y., Yamazaki, T., Koizumi, M., Suga, H., Kusahara, K., Prothro, L., 2016. Widespread collapse of the Ross ice shelf during the late Holocene. Proc. Natl. Acad. Sci. USA 113, 2354–2359.
- You, C.-F., Lee, T., Li, Y.-H., 1989. The partition of Be between soil and water. Chem. Geol. 77, 105–118.
- Zachos, J.C., Kump, L.R., 2005. Carbon cycle feedbacks and the initiation of Antarctic glaciation in the earliest Oligocene. Global Planet. Change 47, 51–66.
- Zerathe, S., Blard, P.-H., Braucher, R., Bourlès, D., Audin, L., Carcaillet, J., Delgado, F., Benavente, C., Aumaître, G., Keddadouche, K., 2017. Toward the feldspar alternative for cosmogenic 10Be applications. Quat. Geochronol. 41, 83–96.